Separation and Purification Technology 329 (2024) 125156

Contents lists available at ScienceDirect

Separation and Purification Technology

journal homepage: www.elsevier.com/locate/seppur

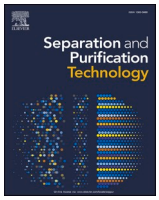

Testing carbon structures for metal-free catalytic/photocatalytic ozonation to remove disinfection by-product formation potential

M.A. Jiménez-López [a,b], A. Rey [a,b,*], V. Montes [b,c], F.J. Beltrán [a,b]

[a] Departamento de Ingeniería Química y Química Física, Universidad de Extremadura, Av. Elvas s/n, 06006 Badajoz, Spain
[b] Instituto Universitario de Investigación del Agua, Cambio Climático y Sostenibilidad (IACYS), Universidad de Extremadura, Av. Elvas s/n, 06006 Badajoz, Spain
[c] Departamento de Química Orgánica e Inorgánica, Universidad de Extremadura, Av. Elvas s/n, 06006 Badajoz, Spain

ARTICLE INFO

Keywords:
Graphite
Graphene
Graphene oxide
Disinfection by-products
Catalytic ozonation
Photocatalytic ozonation

ABSTRACT

Different graphitic carbon structures were prepared and tested for catalytic and photocatalytic ozonation of the precursors of chlorination disinfection by-products to remove their disinfection formation potential (DBPFP). Commercial graphite was submitted to ball milling and two chemical treatments with ammonium nitrate or potassium oxalate to increase its surface area. Additionally, ozonation in gas phase and liquid phase were used to generate surface oxygen groups in these materials and in commercial graphene. All the carbon samples were tested and compared with commercial graphene oxide in the removal of humic acid solutions. The highest catalytic activity during the catalytic/photocatalytic ozonation of humic acid was observed for commercial graphene, ozonated graphene and for graphene oxide; however, this did not result in high DBPFP removal and the instability of the materials was demonstrated. With a moderate catalytic activity but better stability, ball-milled graphite ozonated in liquid phase, was selected for photocatalytic ozonation of real surface water leading to a high DBPFP removal at the conditions tested (88 % 5-HAAs (haloacetic acids), 70 % 4-THMs (trihalomethanes), 70 % AOX (adsorbable organic halides); conditions: semi-batch experiments; 0.5 L volume; 5 mg L^{-1} O_3; Q_g = 10 L h^{-1}; DOC_0 = 5 mg L^{-1}; pH = 7.8; 180 min under simulated solar radiation with average irradiance 580 W m^{-2}).

1. Introduction

Disinfection of drinking water is one of the most important milestones in health protection, eliminating disease-causing viruses and bacteria and thus significantly reducing waterborne illness. Despite these benefits, the formation of disinfection by-products (DBPs) is a consequence of the reaction of disinfectants (chlorine, hypochlorite, chloramines, chlorine dioxide, ozone or UV radiation) with natural (NOM) or anthropogenic organic matter (AOM), bromide or iodide [1,2]. The toxic effects of these DBPs have been in the spotlight since the mid-1970 s after chloroform detection in drinking water treatment plants (DWTPs) and the possible link between different DBPs and some diseases [1,3,4]. Of the more than 700 DBPs identified, among the organics only four trihalomethanes (4-THMs): chloroform, $CHCl_3$; bromodichloromethane, $CHCl_2Br$; dibromochloromethane, $CHClBr_2$; and bromoform, $CHBr_3$; and five haloacetic acids (5-HAAs): monochloroacetic acid, $ClCH_2COOH$; monobromoacetic acid, $BrCH_2COOH$; dichloroacetic acid, $Cl_2CHCOOH$; dibromoacetic acid, $Br_2CHCOOH$; and trichloroacetic acid, Cl_3CCOOH; have been regulated to date but they are not necessarily the most harmful species [1,2]. Besides the commonly analyzed 4-THMs and 5-HAAs, quantification of total organic halides (-Cl, -Br, -I) is a useful tool to check the global amount of halogenated DBPs in drinking water [5].

One of the strategies to reduce the formation of DBPs is to eliminate or transform the precursor organic matter into less reactive species toward chlorine. In this line, advanced oxidation processes (AOPs) have been applied to reduce the formation of DBPs during chlorination [6,7]. Contrarily, it has been observed that AOPs operating with limited energy or chemical inputs can increase DBPs formation due to insufficient concentration/reaction time of hydroxyl radicals (HO·) generated [7]. Ozone has been widely used in drinking water treatment, with ozone exposure playing a key role in the degradation of organic precursors [8,9]. Ozone itself can fast-react with electron-rich sites of NOM, decreasing the nucleophilic sites for chlorine reactions and consequently

* Corresponding author at: Departamento de Ingeniería Química y Química Física, Instituto Universitario de Investigación del Agua, Cambio Climático y Sostenibilidad (IACYS), Universidad de Extremadura (UEX), Avda. Elvas s/n, 06006 Badajoz Spain.
E-mail address: anarey@unex.es (A. Rey).

https://doi.org/10.1016/j.seppur.2023.125156
Received 11 July 2023; Received in revised form 14 September 2023; Accepted 19 September 2023
Available online 22 September 2023

Table 1
Simplified general reactions of ozonation processes for DBPFP removal and DBPs formation.

Ozonation (direct and indirect reactions)	Reference
(1) $O_3 + DOC_0 \rightarrow DOC_i + H_2O_2$	[2]
(2) $O_3 + HO^- \xrightarrow{[\cdots]} HO^{\hat{A}\cdot}$	
(3) $H_2O_2 \leftrightarrows HO_2^- + H^+$; pK = 11.3	
(4) $HO_2^- + O_3 \xrightarrow{[\cdots]} HO^{\hat{A}\cdot}$	
(5) $HO^{\hat{A}\cdot} + DOC_0 \rightarrow DOC_i$	
(6) $HO^{\hat{A}\cdot} + DOC_i \xrightarrow{[\cdots]} CO_2 + H_2O$	
Catalytic ozonation with carbon materials	**Reference**
(7) $O_3 + C_{CAT} \xrightarrow{[\cdots]} HO^{\hat{A}\cdot} + C_{CAT}$	[2]
(8) $O_3 + C_{CAT} \leftrightarrows O_3 - C_{CAT}$	
(9) $DOC_0 + C_{CAT} \leftrightarrows DOC_0 - C_{CAT}$	
(10) $O_3 - C_{CAT} + DOC_0 - C_{CAT} \rightarrow C_{CAT} + DOC_i + H_2O_2$	
(11) $H_2O_2 + C_{CAT} \leftrightarrows H_2O_2 - C_{CAT}$	
(12) $H_2O_2 - C_{CAT} + O_3 - C_{CAT} \rightarrow HO^{\hat{A}\cdot} + C_{CAT}$	
And reactions (1)–(6)	
Photolytic ozonation (simulated solar radiation)	**Reference**
(13) $O_3 + h\nu_{<390nm} + H_2O \rightarrow HO^{\hat{A}\cdot} + H_2O_2$	[16]
And reactions (1)–(6)	
Photocatalytic ozonation	**Reference**
(14) $C_{CAT} + h\nu \rightarrow h^+_{VB} + e^-_{CB}$	[11,17]
(15) $e^-_{CB} + O_2 \rightarrow O_2^{\hat{A}\cdot -}$	
(16) $e^-_{CB} + O_3 \rightarrow O_3^{\hat{A}\cdot -}$	
(17) $O_3 + O_2^{\hat{A}\cdot -} \rightarrow O_3^{\hat{A}\cdot -} + O_2$	
(18) $O_3^{\hat{A}\cdot -} + H_2O \xrightarrow{[\cdots]} HO^{\hat{A}\cdot}$	
(19) $h^+_{VB} + H_2O \rightarrow HO^{\hat{A}\cdot} + H^+$	
And reactions (1)–(13)	
Chlorination	**Reference**
(20) $DOC_0 + HClO/ClO^- \rightarrow DBPs$	[2]
(21) $DOC_i + HClO/ClO^- \rightarrow NoDBPsformation$	

decreasing the formation of THMs and HAAs [8]. However, the maximum mineralization of NOM/AOM achievable by single ozonation is usually low due to the formation of oxidation by-products refractory to ozone attack [10], which can be precursors of other non-regulated DBPs. The hybrid processes combining ozone with a catalyst, radiation, or both, i.e., catalytic ozonation, photolytic ozonation, and photocatalytic ozonation, have been investigated to improve the use of ozone for NOM or humic acid degradation through the generation of higher concentrations of HO· [2].

The activity of carbonaceous materials for catalytic/photocatalytic ozonation is well known, with activated carbon being the most studied [11]. Graphene-based materials offer promising characteristics like high surface areas, electron conducting character, and tunable oxidation degree that can promote the formation of HO· through ozone decomposition [12]. In addition, graphene and its derivatives can act as independent solar-driven photocatalysts depending on their characteristics [13]. As a more environmentally friendly and economic material, high surface area graphite has demonstrated its activity during ozonation, mainly when surface oxygen groups are incorporated at the edge of graphene planes [14]. These materials have rarely been investigated for DBPs' precursors elimination through catalytic ozonation [2]. In addition, modified Fe-TiO_2 has been the only catalyst studied in the photocatalytic ozonation of humic acid [15]. The use of carbon structures adds the advantage of being catalysts free of transition metals, whose leaching must be avoided for drinking water treatment. Table 1 summarizes the main simplified reactions for ozonation, catalytic ozonation and solar assisted ozonation processes for DBPFP removal, with the DBPs formation upon chlorination. In these reactions DOC_0 represents the initial organic matter, DOC_i the intermediate organic compounds formed upon oxidation, with less DBPFP, and *[…]* indicates several steps to reach the final products of any reaction (n).

Therefore, the aim of this work focuses on the comprehensive study of the properties of different carbon structures based on graphite, milled graphite, graphene, and their corresponding oxidized materials by means of ozone, tested as metal-free catalysts for catalytic and solar photocatalytic ozonation to reduce the DBPs formation potential (DBPFP). Thus, a dual role of ozonation has been studied both to generate surface oxygen groups in carbonaceous materials [18–20], and to remove the organic precursors of chlorination DBPs. The materials were tested in the removal of humic acid (one of the main components of NOM) and NOM of real surface water with the final objective of removing the DBPFP by analyzing 4-THMs, 5-HAAs and adsorbable organic halides (AOX) after chlorination. The stability, catalytic activity and real applicability of the tested catalysts are fully discussed.

2. Experimental

2.1. Chemicals and surface water

Ultrapure Milli-Q® water (resistivity 18.2 MΩ cm) from Integral 5 system of Millipore was used for the preparation of all solutions. Humic acid sodium salt technical grade (Sigma-Aldrich, CAS: 68131-04-4), sodium carbonate anhydrous (99.5 wt%, PanReac AppliChem CAS: 497-19-8), nitric acid (65 wt%, Fischer Scientific, CAS:7697-37-2), sulfuric acid (>96 wt%, PanReac AppliChem, CAS:7664-93-9), Sodium hypochlorite (NaClO, 13 % active chlorine, CAS: 7681-52-9), hydrochloric acid (HCl, 37 wt% CAS: 7647-01-0), sodium hydroxide (NaOH, >98 wt% CAS: 1310-73-2), phosphate potassium salts (K_2HPO_4 CAS: 7778-77-0, KH_2PO_4 CAS: 7758-11-4), o-phosphoric acid (H_3PO_4, 85 wt % CAS: 7664-38-2), all from PanReac were used without further purification. Other reagents were of at least reagent grade.

Standards and reagents for DBPs analyses: chloroform (99.8 wt% $CHCl_3$, CAS: 67-66-3), dichlorobromomethane (98 wt% $CHCl_2Br$, CAS:75-27-4), chlorodibromomethane (98 wt% $CHClBr_2$, CAS: 124-48-1), bromoform (99 wt% $CHBr_3$, CAS: 75-25-2), monochloroacetic (99 wt% $ClCH_2COOH$, CAS: 79-11-8), monobromoacetic (99 wt% $BrCH_2COOH$, CAS:79-08-3), dichloroacetic (99.4 wt% $Cl_2CHCOOH$, CAS: 79-43-6), trichloroacetic (99 wt% Cl_3CCOOH, CAS: 76-03-9) and dibromoacetic acids (97 wt% $Br_2CHCOOH$, CAS: 631-64-1); 1,2-dibromopropane (98 wt% CAS: 78-75-1), tetrabutylammonium hydrogensulfate (TBA-HSO_4, CAS: 32503-27-8); dimethyl sulfate (99 wt% DMS, CAS: 77-78-1) and n-pentane (99 wt% CAS: 109-66-0), were supplied by Merck. Methyl *tert*-buthyl ether HPLC-grade (99.8 wt% CAS: 1634-04-4) was supplied by Panreac.

Raw surface water was collected from the Supply Conduction on the Left Bank of the Zújar and Guadiana Rivers (CAMI) located in the province of Badajoz (Spain) in winter 2022. The samples were filtered through paper filters (Whatman Grade 1), analyzed and stored at −20 °C until further use.

2.2. Carbon materials

Graphite (CAS: 7782-42-5) in fine powder (particle size < 20 μm) supplied by Sigma-Aldrich was used as received.

Commercial graphene nanoplatelets from Sigma-Aldrich (CAS: 7782-42-5) were used as received. Its main characteristics according to the supplier were particle size < 2 μm, thickness few nm, specific surface area 750 $m^2\ g^{-1}$.

Graphene oxide was supplied by Graphenea in powder form, with main characteristics: particle size: 90 % of particles < 25–28 nm; 50 % of particles < 13–15 nm; 10 % of particles < 6–7 nm; specific surface area > 100 $m^2\ g^{-1}$, oxygen content 41–50 %.

2.2.1. Treatments to increase the surface area of graphite

Ball milling (BM): commercial graphite was submitted to dry ball milling in a planetary ball mill Pulverisette 6 (Fritsch GmbH). After preliminary tests, the conditions used were ambient atmosphere, 1.5 g of graphite, 14 agate balls of 5 mm, ball to powder ratio 13:1, rotation frequency 600 min^{-1}, beaker volume 80 mL and milling time 16 h. This

Table 2
Samples of carbon materials for catalytic screening.

Starting material	Treatment for surface area	Ozonation	Nomenclature
Graphite	–	–	G_p
Graphite	–	LP	G_p-LP
Graphite	–	GP	G_p -GP
Graphite	BM	–	G_p -BM
Graphite	BM	LP	G_p -BM-LP
Graphite	BM	GP	G_p -BM-GP
Graphite	KO	GP	G_p -KO-GP
Graphite	AN	GP	G_p -AN-GP
Graphene	–	–	G
Graphene	–	LP	G-LP
Graphene	–	GP	G-GP
Graphene oxide	–	–	GO

treatment can lead to the synthesis of graphene-type materials with surface oxygen groups formation and increased surface area [21].

Potassium oxalate treatment (KO): commercial graphite was mixed in a mortar with potassium oxalate in a mass ratio of 1:3 From this mixture, 5 g were placed in a crucible boat in a ceramic horizontal furnace. After sealing, a flow of 100 mL min^{-1} of N_2 was set and the temperature increased to 800 °C at a rate of 10 °C min^{-1} and kept at 800 °C for 30 min before the furnace was stopped and the system was cooled down. Finally, the treated material was washed in a filtration system with 1 L of water to remove all potassium salts formed during thermal treatment.

Ammonium nitrate treatment (AN): 1 g of commercial graphite was mixed with 3 g of ammonium nitrate (mass ratio of 1:3) and 2 mL of MilliQ water under magnetic stirring for 60 min and then the mixture was dried overnight at 40 °C. The mixture was thermally treated in ceramic horizontal furnace under 100 mL min^{-1} N_2 flow. The temperature was increased at 1 °C min^{-1} up to 400 °C, then the power was switched off and the system cooled down. Notice that some explosions were detected during the experiment with heating rate higher than 1 °C min^{-1}, particle size smaller than 63 μm, and N_2 flow lower than 100 mL min^{-1}.

2.2.2. Generation of surface oxygen groups by ozonation

Commercial graphene, commercial graphite, and treated graphite to increase surface area were subjected to ozonation to increase their surface oxygen groups. In general, two procedures in liquid and gas phases were carried out. For liquid phase ozonation (LP), 1.5 g of the material was placed in suspension in 0.5 L of ultrapure water and submitted to a continuous oxygen/ozone flow at 20 L h^{-1} with 80 mg L^{-1} O_3 concentration during 2 h in a semi-batch reactor at ambient temperature. The experimental setup is shown in **Figure S1** of the supplementary information (SI). The ratio of ozone fed per g of carbon material was 2.2 g O_3/g C. After the treatment, the oxidized material was separated by filtration and then dried at ambient temperature. No significant weight loss was observed. For gas phase ozonation (GP), 0.5 g of the material was placed in a U-shaped glass reactor and submitted to a continuous oxygen/ozone flow at 40 L h^{-1} with 60 mg L^{-1} O_3 concentration, during 0.5 h. **Figure S2** shows a scheme of the experimental setup. In this case 2.4 g O_3/g C ratio was used, and a 9 % of weight loss was observed. Table 2 summarizes the materials, their modifications and nomenclature used in this work.

2.3. Characterization analyses

Nitrogen adsorption–desorption isotherms were acquired at −196° in an Autosorb iQ2-C Series apparatus (Quantachrome). Before the analysis, the samples were outgassed at 150 °C for 12 h under a residual pressure $< 10^{-4}$ Pa. BET and t-plot methods were applied to calculate the specific surface area and micropore volume, respectively.

The structural characterization of the samples was carried out by X-ray diffraction and Raman spectroscopy. XRD patterns were collected using a powder Bruker D8 Advance XRD diffractometer with a Cu Kα1 radiation (λ = 1.541 Å) and a linear detector VANTEC (aperture 3°). The data were collected from 2θ = 5–80° at a scan rate of 0.02° s^{-1} and 0.5 s per point. Raman spectra were acquired using an excitation laser source with λ = 630 nm on a Thermo Scientific Nicolet Almega XR dispersive Raman spectrometer.

For surface characterization, Fourier-transformed infrared spectroscopy (FTIR) was carried out using KBr pellet method on a Nicolet iS10 spectrometer. The sampling resolution was 1 cm^{-1} and 32 scans from 400 to 4000 cm^{-1} wavenumber range. In addition, thermal gravimetry and differential temperature analysis coupled mass spectrometry (TGA-DTA-MS) was performed with a STA 449 F3 Jupiter (Netzsch) coupled to a mass spectrometer (QMS 403D Aëolos III from Netzsch) to quantify the evolution of CO_2, CO and H_2O during the temperature programmed treatments. Experiments were carried out in inert (temperature programmed desorption (TPD) in Ar) with a flow rate of 100 mL min^{-1}, using a heating rate of 10 °C min^{-1} from 40 °C to 1100 °C. The pH of the carbonaceous materials slurry (pH_{slurry}) can be equivalent to the pH of the point of zero charge (pH_{PZC}) under certain conditions. The pH_{slurry} was determined by mass titration with 5 wt% carbon loading in ultrapure water as described in the literature in dark conditions and continuous stirring until the pH of the slurry was stabilized [22,23]. Besides, the determination of the pH_{PZC} was carried out for some samples by mass titration through the so-called pH drift method following the stablished procedure in the literature [24,25]. A calibrated pH-meter (Hanna HI12303) was used for pH measurement.

2.4. Catalytic activity tests

Photocatalytic ozonation experiments were conducted in the semi-batch mode using an experimental device schematically shown in **Figure S3**(A) of the SI. A solar box SUNTEST CPS+ (Atlas) equipped with a 1500 W air-cooled Xe lamp working at 550 W m^{-2} (nominal value) and λ > 300 nm was used. The spectral irradiance is shown in **Figure S3**(B) of the SI together with the measured irradiance for UVB, UVA and visible regions, with a measured total irradiance of 581 W m^{-2}. A borosilicate glass spherical reactor with 0.5 L of effective volume was placed in the center of the solar box. In a typical test, the reactor was charged with 0.5 L of the solution of humic acid (HA, 30 mg L^{-1}, 10 mg L^{-1} DOC, pH_0 7) and kept under magnetic stirring. The catalyst was then added to the reactor at a loading of 0.1 g L^{-1} and kept for 30 min agitated in the dark to reach adsorption equilibrium and homogenization. After that, an ozone/oxygen stream produced from pure oxygen by a laboratory ozone generator (Sander Labor-Ozonisator model 301.7) was bubbled at 10 L h^{-1} with 5 mg O_3 L^{-1}. At the same time, the lamp of the solar box was switched on and the oxidation experiment began. The concentrations of ozone in the streams entering and leaving the reactor were continuously monitored. Aqueous samples were withdrawn from the reactor at different times, air bubbled and filtered (0.45 μm syringe filters, Millex®-HA, Millipore) except for dissolved ozone analysis. Samples were analyzed for concentrations of dissolved ozone, dissolved organic carbon (DOC) and hydrogen peroxide. UV–Visible absorbance and pH were also followed. At the end of the experiment, ozone remaining in the reactor was eliminated by air striping and the solution was filtered and reserved for subsequent chlorination.

Catalytic ozonation was also studied using similar procedure but without solar simulator. For comparative purposes blank experiments of photolysis (only radiation), adsorption (only catalyst), ozonation (only ozone), photocatalysis (catalyst and radiation) and photolytic ozonation (ozone and radiation without catalyst) were performed. With a selected catalyst, some experiments were carried out in the presence of carbonate (5×10^{-3} mol L^{-1}) and phosphate (1×10^{-4} mol L^{-1}) and real surface water was also treated. Each experiment was performed at least in duplicate and some of them in triplicate, with an error below 10 % in all cases.

Table 3
Main textural properties of the selected carbon catalysts.

Nomenclature	S_{BET} ($m^2\ g^{-1}$)	S_{MICRO} ($m^2\ g^{-1}$)	S_{EXT} ($m^2\ g^{-1}$)	V_T ($cm^3\ g^{-1}$)	V_{MICRO} ($cm^3\ g^{-1}$)
G_p	6.9	0	6.9	0.09	0
G_p-LP	7.1	0	7.1	0.08	0
G_p -GP	8.0	0	8.0	0.06	0
G_p -BM	66	15	50	0.15	0.009
G_p -BM-LP	95	15	80	0.17	0.007
G_p -BM-GP	80	4.0	76	0.18	0.006
G_p -KO-GP	49	0	49	0.11	0
G_p -AN-GP	4.7	0	4.7	0.07	0
G	760	275	485	1.45	0.144
G-LP	732	269	463	1.16	0.140
G-GP	723	251	472	1.19	0.123
GO	161	17	144	0.25	0.005

2.5. Chlorination

Initial solutions of HA, raw surface water, and the solutions after the oxidation treatments were submitted to chlorination with sodium hypochlorite using a Cl_2/DOC mass ratio higher than 15. Chlorination was carried out at pH 7 in closed glass bottles with effective volume of 150 mL and without headspace. After 24 h in the dark, the chlorination reaction was stopped by removing the remaining chlorine with ascorbic acid and the samples were immediately processed to analyze 4-THMs, 5-HAAs and AOX. At these conditions, in high excess of chlorine, DBP formation potentials were obtained.

2.6. Analytical methods for reaction monitoring

Measurements of pH were made with a pH-meter (Hanna HI12303). Aqueous ozone concentration was measured at 600 nm by the indigo method [26], and hydrogen peroxide formed during the reactions was determined by the cobalt/bicarbonate method [27]. UV–Visible spectra and absorbance at 254 nm (A254) were also recorded and specific ultraviolet absorption at this wavelength was calculated (SUVA). Total phenolic content (TPhC) was analyzed by the Folin-Ciocalteu reagent. All the spectrophotometric measurements were carried out in a Thermospectronic Evolution 201 spectrophotometer (Thermo Scientific) using 1 cm path length cuvettes. Total organic carbon (TOC) and inorganic carbon (IC) from filtered samples (dissolved organic carbon, DOC) were determined on a Shimadzu apparatus (TOC-V CSH model). In the ozonation experiments, the concentrations of ozone in the gas at the inlet and outlet flows of the reactor were continuously monitored with two on-line ozone analyzers (Anseros Ozomat GM-PRO and GM-OEM models).

Commercial chlorine was standardized by measuring the absorbance of ClO^- at 292 nm in a Thermospectronic Evolution 201 spectrophotometer [28]. After chlorination, raw and treated water were analyzed for DBPs. 4-THMs were analyzed by GC-μECD (Agilent 8690 plus) with HS (Agilent HS 7694E) using a HP5-ms UI capillary column (30 m × 0.32 mm × 0.25 μm) and He as carrier gas. 5-HAAs were analyzed in the same GC-ECD-HS system following the method fully described elsewhere [29]. Total adsorbable organic halides (chlorinated, brominated and iodinated organic matter adsorbed onto activated carbon) was measured in an AOX analyzer as μg eq.Cl L^{-1} (AOX-Multi X 2500, Analytik Jena).

3. Results and discussion

3.1. Properties of carbonaceous materials

The porous structure of the carbonaceous materials and the modification produced by the applied treatments were studied by means of N_2 adsorption–desorption isotherms. The main textural parameters are summarized in Table 3 and isotherms are depicted in **Figure S4.**

Attending to the treatment to modify the surface area, bare and ozonated graphites (Gp- samples) showed low values of BET surface area with no microporosity, some mesoporosity is evidenced by the form of the isotherm of these materials with H3 hysteresis loop, according to the IUPAC classification [30]. On the other hand, ball milling treatment (Gp-BM- samples) developed higher specific areas, mainly external surface with mesoporous contribution but also with the generation of some microporosity. These series presented type-IV isotherms with an H3 hysteresis loop [21,30]. Similarly, the oxalate treatment (Gp-KO-GP sample) led to an increase of the BET surface area and total pore volume with no microporosity generation. On the contrary, the ammonium nitrate treatment (Gp-AN-GP sample) did not substantially modify the porous characteristics of bare graphite, showing low surface area and adsorbed pore volume with an isotherm comparable to that of graphite samples. Regarding the graphene series, all the G- samples exhibited a combination between types I and IV isotherms and a H4 hysteresis loop, indicating the existence of micro- and mesoporosity in these materials with the highest surface areas and pore volumes (see values in Table 3) [30]. Graphene oxide (GO) presented an intermediate value of BET surface area with low contribution of microporosity, being graphene planes of small size highly exfoliated and oxidized.

With respect to the ozonation treatments, BET surface areas increased after ozonation for the series of graphite and ball-milled graphite. This increment was produced in the external surface area and was more pronounced for the ball-milled graphite with lower particle sizes, as previously observed [31]. Although in the case of graphene series, BET surface areas and micropore volumes of ozonated samples are lower than in the original graphene as reported for other high-area activated carbons and reduced graphene oxides [32–34]. This is generally related to the possible destruction of some micropore walls and their collapse when oxygenated terminal groups are created and/or to the formation of these groups at the entrance of the micropores [35].

The structure of the materials was analyzed by XRD and Raman spectroscopy. Fig. 1 displays XRD patterns of all samples. Graphite samples (Gp-) showed the (0 0 2) peak at approximately 26.5° attributed to the orientation of the aromatic ring carbon layers in 3D arrangement. Thus, the narrower and the higher the (0 0 2) peak, the better the orientation. The presence of this peak with different intensity and displacement is observed in all the graphite treated samples (Gp-, Gp-BM-, Gp-AN- and Gp-KO- samples) and in graphenes (G-). On the other hand, the XRD pattern of graphene oxide shows its characteristic (0 0 1) peak at 10.5° [36,37]. The interlayer spacing d_{002} (d_{001} for GO) and the staking height (L_c) was calculated as described in the **S.I.** [38], and the values are summarized in Table 4. Ball milling provoked the breakthrough of the graphite particles, lowering the stacking heigh of graphene sheets, when compared L_c in Gp- and Gp-BM- samples, also with some distortion in the distance between graphene sheets as previously reported [21]. Contrarily, no significant distortion of the structural order is observed through the L_c and d_{002} values of both ammonium nitrate and oxalate treated graphite. The subsequent ozonation treatments did not introduce significant modifications in the XRD parameters studied.

First-order Raman spectra of all carbon samples are depicted in Fig. 2 where the characteristic G and D peaks are observed, respectively attributed to in-plane vibrations of the aromatic carbon structure and structural defects or loss of symmetry. The G band located at Raman shift around 1570–1578 cm^{-1} is due to first order scattering from the E_2g mode of sp^2 carbon bonding. The D band located at 1320–1335 cm^{-1} is due to structural defects [21,39,40]. Additional defect-related bands or shoulders (D', D" and D*) have been described for graphitic materials [39]. According to Claramunt et al. (2015) and the references herein [41], the D' band, centered around 1620 cm^{-1}, is attributed to the disorder-induced phonon mode due to crystal defects, but also to double vacancy corresponding to pentagonal and octagonal rings; D" band, located between 1500 and 1550 cm^{-1}, can be attributed to contributions from the phonon density of states in finite-size crystals of graphite or

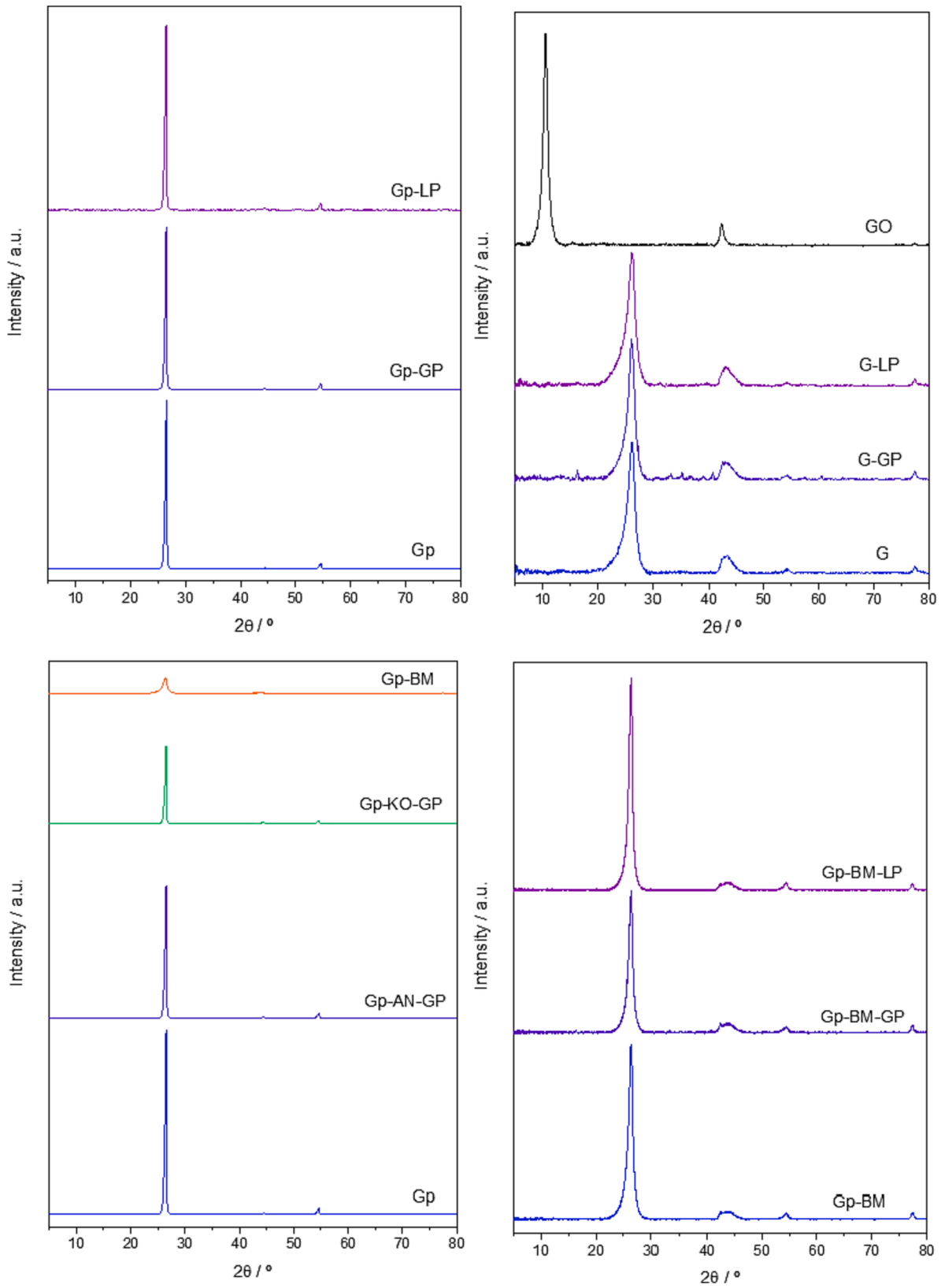

Fig. 1. XRD patterns of carbonaceous materials.

also to amorphous lattices or interstitial defects associated with amorphous sp^2-bonded forms that may include functionalized small molecules; and D* small band, between 1150 and 1200 cm^{-1} has been related with disordered graphitic lattice provided by sp^2-sp^3 bonds at the edges of networks. The spectra were decomposed to calculate the areas of G, D and D' bands according to literature. The deconvolution of the first-order Raman spectra is presented in **Figures S5 and S6**, and the Raman shift of D, G and D' bands, the intensity ratios I_D/I_G and $I_G/I_{D'}$

Table 4
Structural parameters by Raman and XRD analyses.

Nomenclature	XRD parameters			Raman parameters					
	2θ (°)	d_{002} (nm)	L_c (nm)	D (cm^{-1})	G (cm^{-1})	D' (cm^{-1})	I_D/I_G	$I_G/I_{D'}$	L_a (nm)
G_p	26.54	0.336	25.7	1333.0	1576.4	–	0.43	–	87.7
G_p-LP	26.47	0.337	26.4	1330.5	1578.0	–	0.58	–	65.0
G_p -GP	26.49	0.336	27.1	1326.0	1572.6	–	0.43	–	87.4
G_p -BM	26.39	0.338	8.69	1324.3	1577.6	1609.6	2.43	4.52	15.5
G_p -BM-LP	26.39	0.338	10.3	1328.8	1578.4	1609.3	2.49	3.96	15.2
G_p -BM-GP	26.40	0.338	9.23	1323.9	1571.4	1604.2	2.53	2.30	14.9
G_p -KO-GP	26.52	0.336	28.7	1328.2	1575.2	–	0.41	–	92.2
G_p -AN-GP	26.53	0.336	22.7	1330.5	1577.0	1616.8	0.83	30.3	45.3
G	26.29	0.339	5.05	1318.0	1574.0	1605.0	4.39	2.31	8.61
G-LP	26.27	0.339	5.04	1320.3	1571.0	1603.2	4.29	2.21	8.81
G-GP	26.17	0.341	5.98	1320.1	1570.2	1600.5	4.36	1.33	8.67
GO	10.51	0.842	8.36	1335.3	1577.3	1599.5	5.43	1.67	6.96

and the in-plane sp^2 crystallite size (L_a) calculated from I_D/I_G values (see **S.I.**) are summarized also in Table 4.

A more intense G band is observed for untreated graphite (Gp) and ozonated graphite in gas phase, whereas the ozonation in liquid phase increased the defects in the graphitic structure lowering in-plane L_a size (for Gp-LP). After ball milling, the samples presented more intense D bands and broadened G bands with a significant D' shoulder, due to the presence of more defects also characteristic of the presence of few-layered graphene as previously reported [21]. The contribution of this D' band in the Raman spectra was also observed for graphene based materials (G- samples, **Figure S6**). On the other hand, potassium oxalate treatment seems not to change any of the structural parameters observed by Raman whereas ammonium nitrate led to a larger D band with lower L_a value than the original graphite sample (a somewhat lower L_c value was also observed by XRD). In addition, ozonation treatments in liquid or gas phase seem not to modify the I_D/I_G ratio and L_a of ball-milled graphite or graphene samples (Gp-BM- and G samples in Table 4). However, the $I_G/I_{D'}$ ratio decreased with the ozonation treatments in the Gp-BM and G materials. The intensity of the D' band is related to the presence of sp^3 carbon and structural defects produced during oxidation [39,41]. Finally, the parameters observed for graphene oxide agree with those found in the literature [39,42].

Therefore, although no treatment achieved high exfoliation degree of the graphene layers of graphite to form graphene, oxidized graphene or graphene oxide, ball milling led to structural distortion breaking the graphite particles through the in-plane graphene sheets, through the staking height and with graphene layers separation, which also led to an increase of the surface area. This was less significant for potassium oxalate and ammonium nitrate treatments. Besides, although ozonation treatment did not significantly modify the structure of the materials with no changes observed by XRD, the generation of defects for high surface area sample (G- and G-BM- series) was corroborated by Raman spectroscopy.

The oxidation degree achieved with the ozonation treatments was analyzed by FTIR and TPD. Fig. 3 shows the FTIR spectra of all carbon samples. In the analysis of surface functional groups of carbonaceous materials by FTIR some characteristic bands appear. A broad band located at 3000–3500 cm^{-1} corresponds to O–H stretching vibration; at 1750 cm^{-1} the C═O stretching in carbonyl groups can be observed; ca.1600–1650 cm^{-1} C═C in-plane sp^2 carbon, adsorbed water and carbonyl groups conjugated in the graphene layer such as the quinone structure C═O and a small amount of C–C, as well as C–H groups in the surface aromatic structure are described; the band located ca. 1375 cm^{-1} is ascribable to C-OH stretching; at around 1220 cm^{-1} epoxy groups (-O-) have been observed and near 1050 cm^{-1} vibration of epoxy, ether or peroxide groups are reported [19,22,43–45]. It can be highlighted the highest oxidation of graphene oxide, with a large amount of surface oxygen functionalities, mostly –OH and C═O groups (Fig. 3(A)). On the other hand, in general, ozonation treatments increased the presence of these surface oxygen groups with respect to untreated materials (graphene, graphite or ball-milled graphite). Also, gas phase ozonation generated higher amount of surface oxygen groups than liquid phase ozonation for graphite-based materials (Fig. 3(B) and (C)) but not for ozonated graphene (Fig. 3(A)), according to the relative intensity of the bands observed. Ball milling at the conditions used also promoted the generation of surface oxygen structures (Gp vs. Gp-BM samples). This was previously reported for other graphite materials and is attributed to the oxygen of the jar atmosphere during the ball milling procedure especially at long times (16 h for Gp-BM) [21].

Temperature-programmed desorption in inert flow provides information on the nature of surface oxygen groups that decompose upon heating by releasing CO and CO_2 at different temperatures [46]. **Table S1** summarizes the temperature ranges and species detected for different oxygen functionalities. Thus, carboxylic acids, anhydrides, lactone and pyrone-like structures are released as CO_2, whereas anhydrides, phenolic, carbonyl and quinone-like desorb as CO. Fig. 4 shows the TPD curves of selected samples. The total amounts of CO and CO_2 were obtained by integration of the areas under de curves and summarized in Table 5. In addition, the pH_{slurry} and some pH_{PZC} values from selected samples are listed in Table 5. Taking into account the similarities obtained between both values, the discussion about surface acidity will be performed with pH_{slurry} values which, in fact, at the conditions tested with enough carbon load, are equivalent to the pH_{PZC} [22]. The curves for pH_{PZC} determination can be found in **Figure S7**.

The generation of surface oxygen groups during the ball milling of graphite was confirmed by TPD. The profile of CO_2 released indicates some carboxylic acids, anhydrides and lactones. Also an increment of the CO evolving groups was observed. The CO_2-evolving groups are the main responsible for modifying the acidic character of the carbon surface [47]. Thus, a drop in the pH_{slurry} was observed from 6.01 to 5.1 after ball milling. On the other hand, the ozonation treatments of ball-milled samples both in liquid and gas phase, led to an important increase in the CO_2-evolving groups accompanied by a higher acidic character (lower pH_{slurry}). The generation of larger amount of carboxylic acid-type groups during ozonation in liquid phase was observed, giving rise to the highest acid character of the -BM samples. In the case of graphene samples, the starting material (G) presents higher amount of surface oxygen groups, mainly carboxylic acid and anhydride-type. The ozonation led to the surface oxidation with a large amount of CO and CO_2, being also evidenced the preferential generation of carboxylic acid-groups during the treatment in liquid phase. This is reflected in the acidic character of G-LP sample. Regarding graphene oxide, this material shows the typical CO and CO_2 profiles, in which epoxy and hydroxyl groups weakly bonded are reported as the main contribution at lower temperatures, and the subsequent evolution is due to carboxylic, anhydrides, phenolic and quinone-carbonyl groups [45]. The content of CO and CO_2 in GO was the

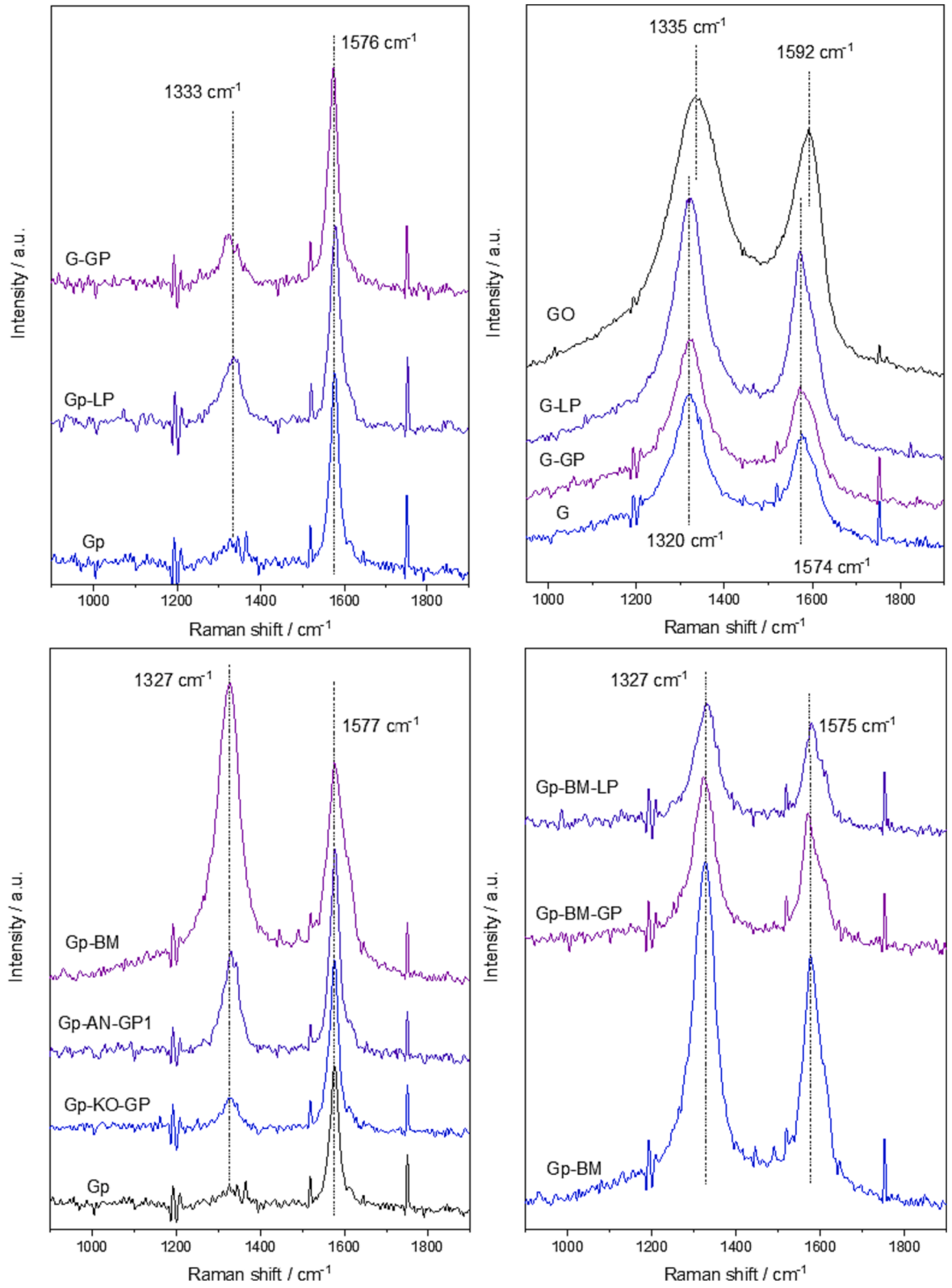

Fig. 2. First-order Raman spectra of carbonaceous materials.

highest of the materials studied and it presented also a highly acidic character with the lowest pH_{slurry} value. It is noteworthy that GO has 45–50 wt% of oxygen in its structure. All these results are consistent with the evidence found by Raman and FTIR.

Therefore, to summarize this part, the ozonation treatment of all carbon materials produced the generation of surface oxygen groups of acidic-type when ozonation is performed in liquid phase in contrast to the generation of more phenolic-like groups through ozonation in gas phase. The increase in the amount of SOG went hand in hand with a higher surface area of the materials.

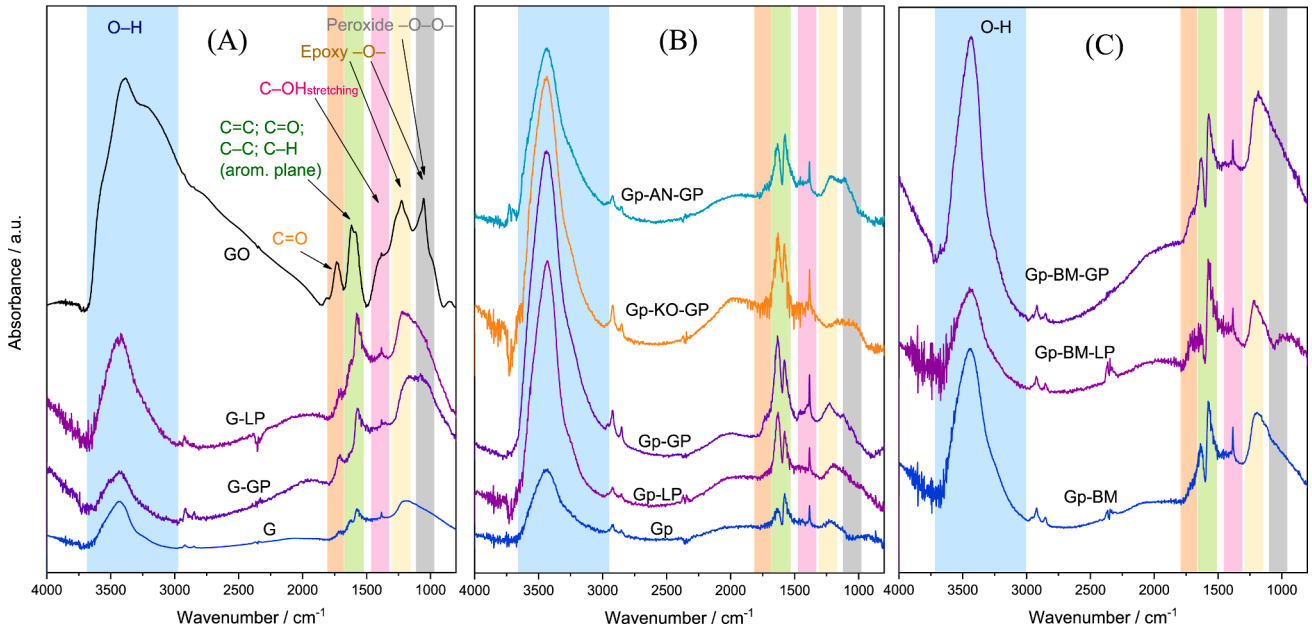

Fig. 3. FTIR spectra of graphene-based and graphene oxide materials (A); graphite-based materials (B); and graphite ball-milled materials (C).

3.2. Screening of carbon materials for the catalytic and photocatalytic ozonation of humic acid and removal of disinfection by-products formation potential

With the purpose of pre-selecting some active materials among the carbon catalysts, in a first step the degradation of a humic acid solution has been studied in catalytic and photocatalytic ozonation treatments. After oxidation, final water samples were submitted to chlorination and then trihalomethanes, haloacetic acids and AOX formation potentials (THMFP, HAAFP, AOXFP) were measured and used also as decision parameters to select the materials. Blank experiments of photolysis and photocatalytic oxidation without ozone demonstrated negligible DOC removal with no important modification in the DBPFP (results not shown), which point out the low photocatalytic activity of the materials under solar radiation in the absence of ozone.

First, noted that regarding the DBPs formed upon chlorination of commercial humic acid solution, the highest concentrations were quantified for chloroform (CF), dichloroacetic (DCA) acid, and trichloroacetic acid (TCA) which account for 75 % of total AOX.

On the other hand, for ozonation treatments, Fig. 5 shows the percentages of DOC removal and the subsequent elimination of disinfection by-products formation potential (DBPFP) after chlorination of the treated samples. Additionally, the DOC evolution with time for all the treatments is presented in **Figure S8.** In general, from de profiles, the catalytic activity of the materials was low to moderate when the results of single ozonation or photolytic ozonation were compared with the catalytic reactions for DOC removal, although the presence of radiation improved the DOC and DBPs elimination.

During single ozonation, the lowest DOC removal (30 %) was observed but the formation of DBPs dropped with 75 % THMFP, 67 % HAAFP and 28 % AOX eliminations compared to DBPs formed upon chlorination of humic acid initial solution. When radiation is applied (O_3/rad or photolytic ozonation), the generation of hydroxyl radicals can be improved accelerating the decomposition of ozone [16]. At the conditions used DOC removal increased up 42 % for photolytic ozonation compared to ozone alone, though this was not reflected in better DBPs results. In fact, THMFP removal decreased up 67 % and AOXFP elimination dropped up 4 %. Only HAAFP removal increased by 86 %. During oxidation treatments, the nature of the organic matter changes to form other intermediates before mineralization to CO_2 and H_2O, and the different structures will have different reactivity with chlorine and, as a consequence, will affect the type and concentration of DBPs formed upon chlorination [48]. Then, ozone itself was the main responsible on the elimination of THMs precursors (mainly humic and fulvic acids) whereas hydroxyl radicals may improve the removal of other DBPs precursors [2,8,48–50].

The use of graphite (Gp and ozonated Gp-LP, and Gp-GP) as catalysts for ozonation demonstrated a poor behavior for Gp and Gp-LP samples, with DOC removal somewhat higher than ozone alone but with the increase of concentrations of 4-THMs and AOX. Only for HAAs the removal of precursors seems to be improved. However, the sample Gp-GP showed better performance with the highest DOC, THMs and AOX elimination of the series. It is noteworthy that the differences are small, with DOC removal (**Figure S8**) or DBPFP elimination only 5–10 % higher than for single ozonation, indicating the low activity of this material. Better results were observed when radiation was applied with Gp-GP material except for THMFP removal due to the lowest ozone concentration available for humic acid direct ozonation. The null AOX removal or even the formation of higher concentrations of AOX than that of the raw humic acid solution when Gp and Gp-LP materials are used can be related to the partial transformation of humic acid in substances with a different AOXFP or also to the release of some organic moieties from carbon structures. The main differences in Gp-GP with respect to the rest of its series is a higher –OH-type SOG detected by FTIR and a slightly lower pH_{slurry}. These surface oxygen groups may play an important role in the ozone decomposition into reactive species in carbon materials, but also favor the hydrophilicity and the Gp-GP water dispersion, improving then its performance [14].

Regarding the behavior of graphites with expanded area, in general, the best results in catalytic ozonation were observed for Gp-BM with 41 % DOC removal, and 77, 86 and 30 % THMFP, HAAFP and AOXFP elimination, respectively. For AOXFP, the rest of the materials of this series presented lower removals than single ozonation or even higher AOXFP than raw humic acid. Under radiation, the results were improved, showing the catalyst Gp-BM-LP the best performance in almost all parameters evaluated also with the highest AOXFP removal (66 %). Additionally, it is noticeable the behavior of ammonium nitrate-graphite (Gp-AN-GP). From these results compared with the homologous in Gp-series, surface area in this range (7–80 $m^2\ g^{-1}$) does not play a key role for the treatments at the conditions used, but the formation of

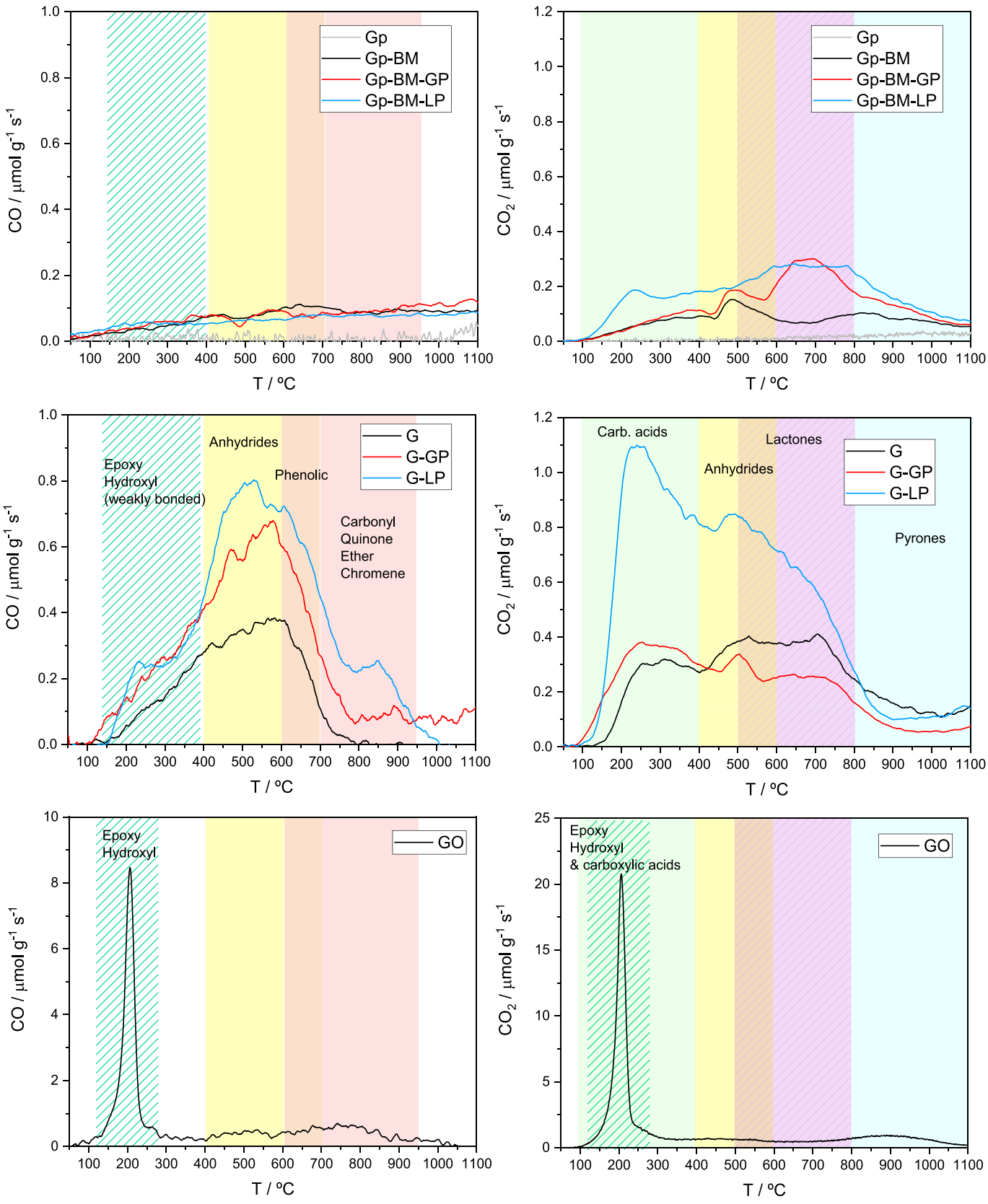

Fig. 4. CO and CO_2 evolution during TPD analyses.

Table 5
Total CO and CO_2 evolved from the TPD, pH_{slurry} and pH_{PZC} of some carbon samples.

Nomenclature	CO (μmol g^{-1})	CO_2 (μmol g^{-1})	pH_{slurry}	pH_{PZC}
G_p	0	0	6.01	6.7
G_p-LP	–	–	5.79	–
G_p -GP	–	–	5.52	–
G_p -BM	463	453	5.1	5.7
G_p -BM-LP	418	1041	3.67	–
G_p -BM-GP	486	786	4.03	–
G_p -KO-GP	–	–	3.81	–
G_p -AN-GP	–	–	6.24	6.3
G	754	1473	4.43	3.5
G-LP	1495	3153	3.87	3.1
G-GP	1585	1237	4.38	–
GO	3462	7013	1.85	1.1

SOG seems to benefit the catalytic activity.

Finally, with respect to the use of graphene or graphene oxide as catalysts, it is noteworthy the highest DOC removal rate (**Figure S8**) and percentage of DOC removal obtained with GO during catalytic ozonation with the highest THMFP and HAAFP elimination (Fig. 5). However, degradation of the GO material was observed during the experiment. As the experiment proceeds, it becomes very difficult to filter the sample, which could indicate the degradation of the GO particles to much smaller sizes which will be detrimental to the separation and reutilization, and finally resulting in the loss of the catalyst. In addition, the final AOX value was higher than that for the initial humic acid solution, likely indicative of the formation of some by-products from GO ozonation able to react with chlorine. The decomposition of GO into humic-like and other organic moieties upon prolonged water contact and ozonation was previously reported [51,52]. In photocatalytic ozonation, under more severe oxidizing conditions, the DOC removal observed using GO was much lower than during dark ozonation and the instability of the material was also evidenced. On the other hand, the use of graphene and oxidized graphene samples led to the best results in terms of mineralization both in dark and photocatalytic ozonation. This can be related to the degree of structural distortion in these materials which in fact, makes them rich in active sites for ozone decomposition. Also, a beneficial effect of the large surface area of graphene (>700 m^2 g^{-1}) cannot be discarded compared to the other carbon catalysts. Regarding DBPs, the elimination of THMFP and HAAFP was also high, but this did not result in much higher elimination of AOXFP. In fact, the percentage of AOX quantified as THMs (mainly CF) or HAAs (DCA and TCA) dropped to ca. 15 %, showing a higher contribution of other DBPs. Of this G-series, G-LP showed the best performance with the highest content of SOG.

Considering these results, it is difficult to establish straightforward relationships between textural, structural and surface properties with the catalytic activity of the materials in photocatalytic ozonation.

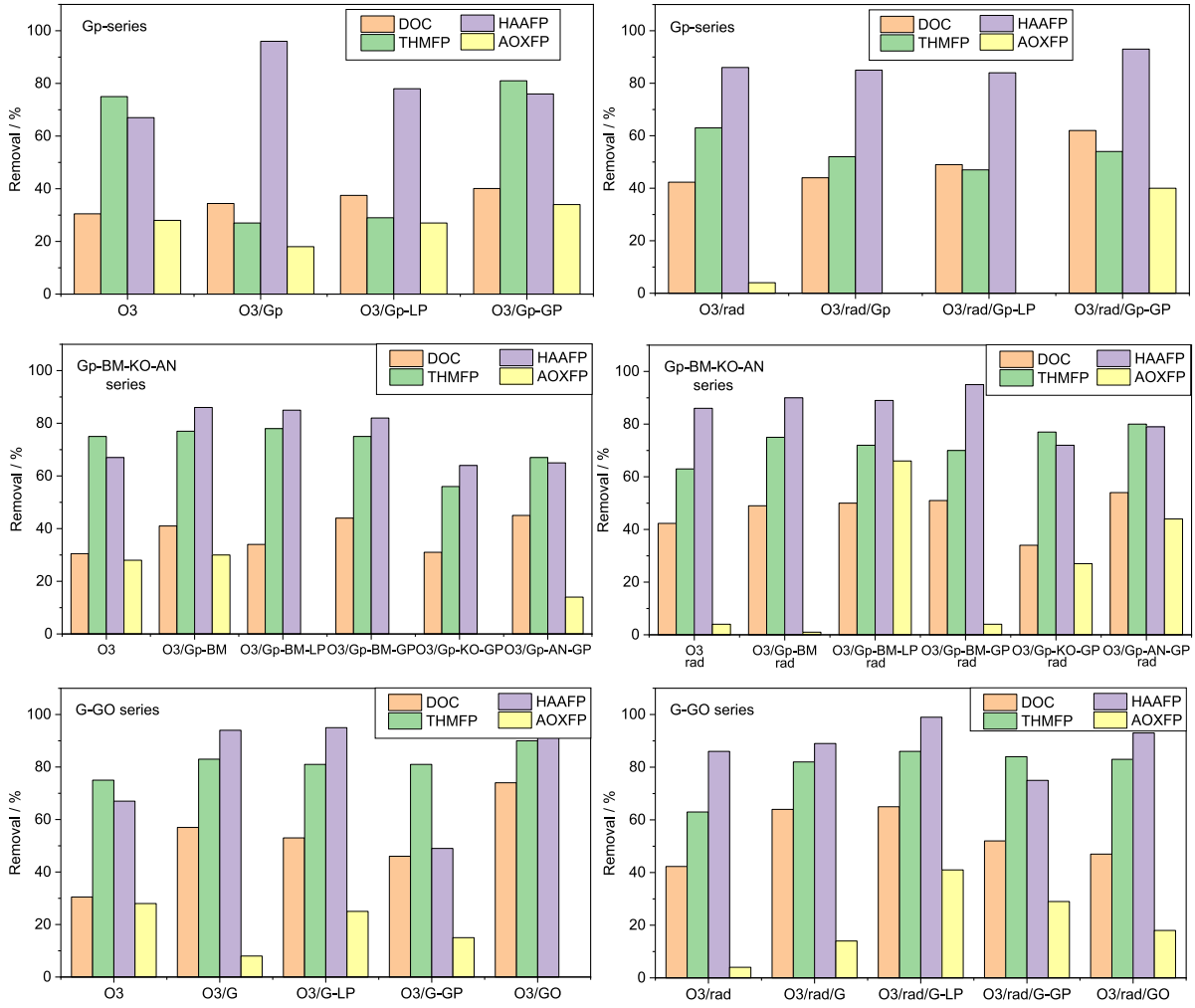

Fig. 5. DOC removal after 90 min of ozonation treatment and postchlorination DBPFP elimination. Ozonation conditions: $C_{HA,0}$ = 30 mg L^{-1}; DOC_0 = 10 mg L^{-1}; C_{CAT} = 100 mg L^{-1}; C_{O3g} = 5 mg L^{-1}; Q = 10 L h^{-1}; pH_0 = 7; I_{irr} = 581 W m^{-2}; V = 0.5 L. Chlorination conditions: V = 125 mL; pH = 7; Cl_2/DOC > 15 mg/mg; $THMFP_0$ = 1130 μg L^{-1}; $HAAFP_0$ = 1906 μg L^{-1}; $AOXFP_0$ = 2840 μg eq. Cl L^{-1}.

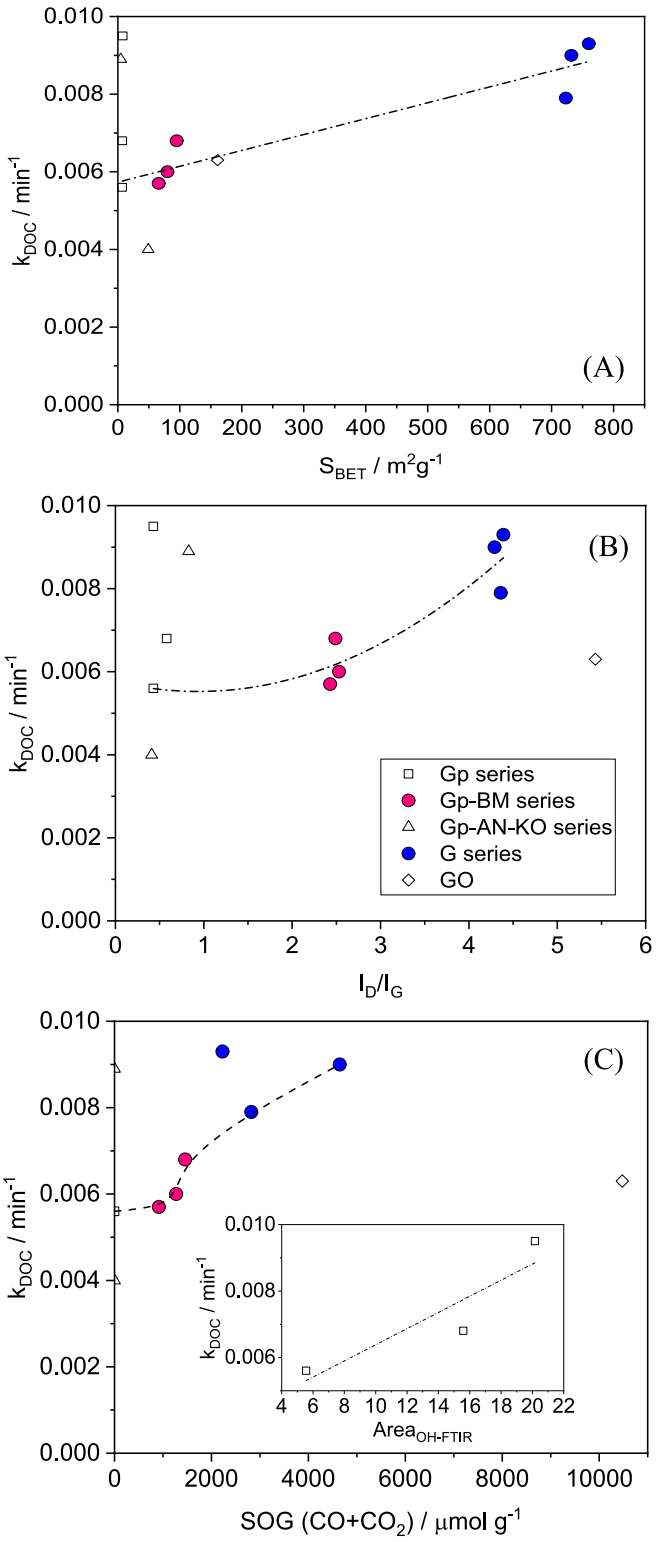

Fig. 6. Apparent k_{DOC} rate constant of photocatalytic ozonation of HA (similar conditions than in **Figure S8**) vs. BET surface area (A); Raman I_D/I_G structural ratio (B); and total SOG content from TPD or –OH peak area from FTIR (C).

However, some general trends can be observed for each series with some exceptions. The apparent first-order rate constant of DOC depletion (k_{DOC}) during photocatalytic ozonation has been calculated and the values are summarized in **Table S2** (see supplementary information). Fig. 6 shows the relationship between the calculated rate constants and some properties of the carbon catalysts.

From Fig. 6**(A)** a positive effect of the increase of BET surface area in k_{DOC} is observed with an almost linear trend, except for ozonated graphite in which the generation of SOG can play an important role. Notice that Gp samples have the lowest BET surface area and the highest order degree of the graphite structure. Also, the carbon structures thermochemically treated to increase the surface area (-AN and -KO samples) show a different behavior. On the other hand, the importance of the degree of distortion in the graphitic structure has been analyzed through the I_D/I_G ratio obtained by Raman spectroscopy (Fig. 6**(B)**). In general, a high ratio of structural defects or disordered carbon favors an increment in the photocatalytic activity except for ozonated graphite, -AN/-KO samples and also for GO. In this case, graphene oxide showed an unstable behavior with the release of DOC to the irradiated reaction medium which did not occur in dark ozonation. Finally, the importance of the concentration of surface oxygen groups has been evaluated in Fig. 6**(C)**. The total amount of SOG has been calculated as CO + CO_2 evolved upon heating in TPD analyses. In addition, for graphite and ozonated graphite (Gp- series), the area of –OH band in FTIR has been used (Fig. 6**(C)**, embedded). Generally, the amount of SOG shows a positive effect in the catalytic activity of the materials. This effect is clearly observed for ozonated graphite with a very low surface area and a very low structural distortion degree. These observations agree with previous studies in which the generation of structural defects in graphitic materials are hand in hand with BET surface area increase, being these sites also centers able to generate SOG upon oxidation treatments and able to favor ozone decomposition in reactive oxygen species such as OH· [14,19,32,35].

However, in terms of DBPs formation potential removal, i.e. the degradation of the precursors of chlorination DBPs, a direct link cannot always be established between the elimination rate of DOC and AOXFP as observed in **Figure S9**. From these results, considering DOC but also DBPFP removal, stability and costs (note that laboratory prices from the suppliers indicate that graphene and graphene oxide are about 12 and 900 times more expensive than graphite, respectively), the next studies were carried out using ball-milled graphite ozonated in liquid phase (Gp-BM-LP).

3.3. Checking Gp-BM-LP's performance on photocatalytic ozonation for DBPFP removal

Fig. 7 shows the evolution of DOC (A), SUVA (B), pH (C) and TPhC (D) during ozonation of humic acid solutions using the material Gp-BM-LP for the catalytic treatments. From DOC evolution, although the catalytic/photocatalytic activity of the material is moderate to low, the best results are observed for photocatalytic ozonation. On the other hand, it has been usually observed that pH drops during ozonation of organic compounds due to the formation of short-chain organic acids as intermediates (see pH in Fig. 7**(C)**).

Ozone decomposition in liquid phase is promoted at high pH into reactive species like HO·, but at the same time, the improvement of ozonation by the use of a catalyst or radiation to promote HO· formation is usually greater at acidic pH values [16]. Then, to check the effect of pH and the importance of hydroxyl radicals during photocatalytic ozonation additional experiments have been carried out at constant pH 7 using a phosphate-buffered solution and also in the presence of carbonate/bicarbonate ions (equivalent to 60 mg L^{-1} IC), a known HO· scavenger for ozonation reactions. It can be observed in Fig. 7**(A)** that humic acid mineralization was quite similar during photolytic ozonation regardless of the constant pH and the presence of carbonate/bicarbonate ions, indicating that other species rather than HO· can be generated through the combination of ozone and radiation improving HA degradation [16]. On the other hand, the presence of the catalyst accelerates the DOC removal to some extent, but similar conclusions are reached with respect to pH and carbonates at the conditions used in this work. In fact, DBPFP removal was similar at pH 7 regardless of the presence of carbonates (see Fig. 8).

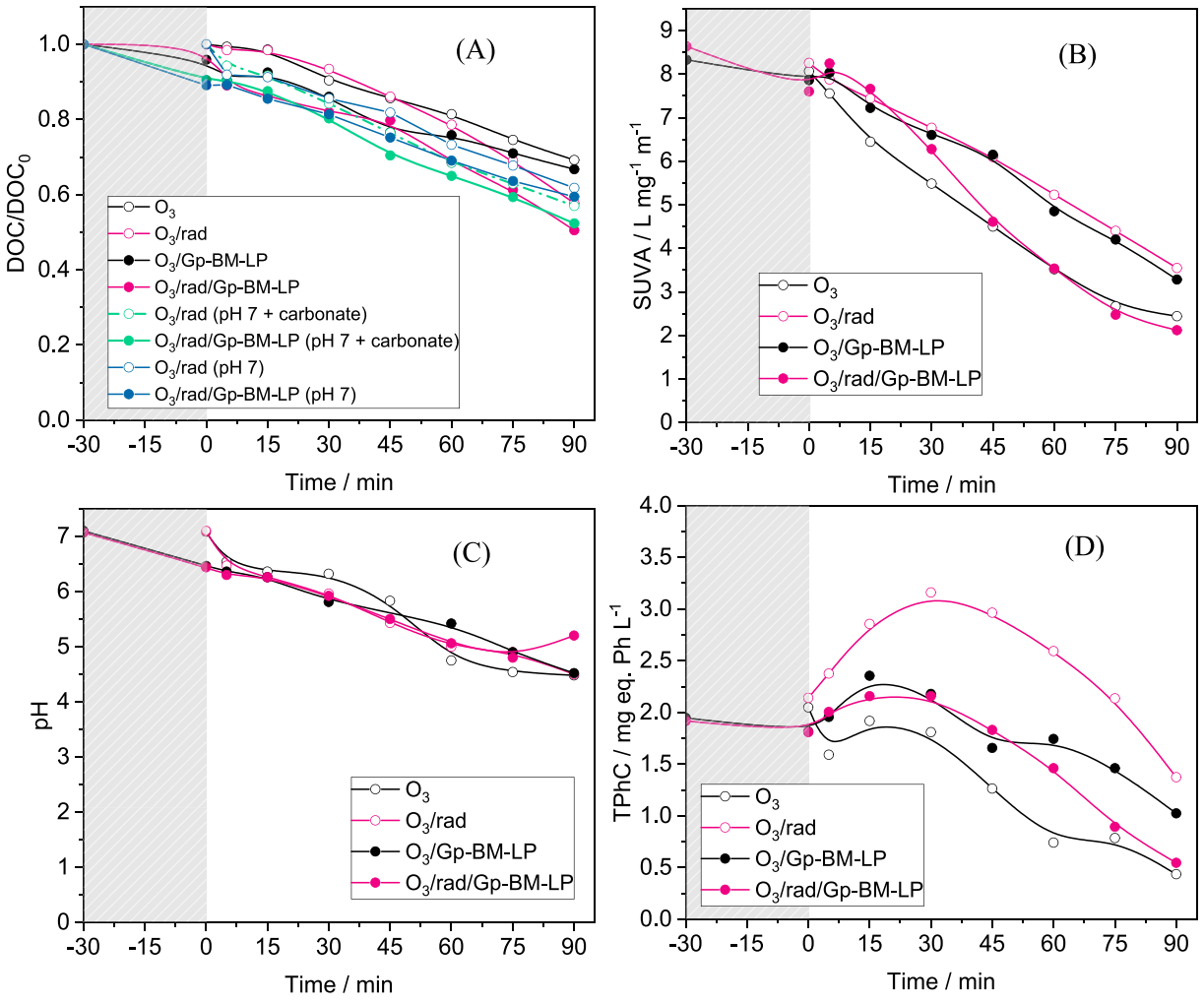

Fig. 7. DOC, SUVA, pH and TPhC evolution during ozonation treatments with Gp-BM-LP catalyst. Ozonation conditions: $C_{HA,0}$ = 30 mg L^{-1}; DOC_0 = 10 mg L^{-1}; $SUVA_0$ = 8.5 L mg^{-1} m^{-1}; $TPhC_0$ = 1.9 mg eq. phenol L^{-1}; C_{CAT} = 100 mg L^{-1}; C_{O3g} = 5 mg L^{-1}; Q = 10 L h^{-1}; pH_0 = 7; I_{irr} = 581 W m^{-2}.

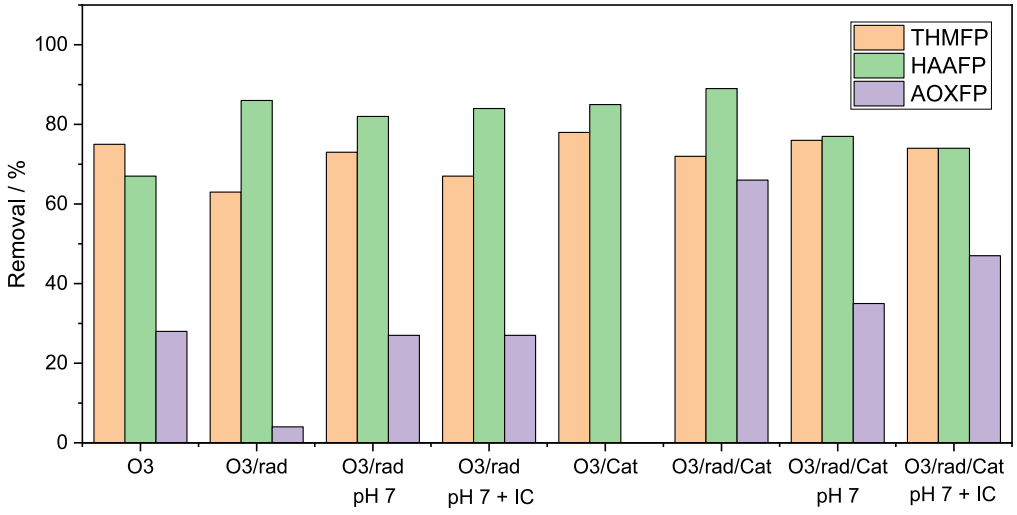

Fig. 8. Postchlorination DBPFP elimination in 90-min treated samples by ozonation. Ozonation conditions: $C_{HA,0}$ = 30 mg L^{-1}; DOC_0 = 10 mg L^{-1}; C_{CAT} = 100 mg L^{-1}; C_{O3g} = 5 mg L^{-1}; Q = 10 L h^{-1}; pH_0 = 7; *Buffered runs pH = 7 ($C^{3-}_{PO4} = 1 \times 10^{-4}$ mol L^{-1} $C^{2-}_{CO3} = 5 \times 10^{-3}$ mol L^{-1}); I_{irr} = 581 W m^{-2}; V = 0.5 L. Chlorination conditions: V = 125 mL; pH = 7; Cl_2/DOC > 15 mg/mg; $THMFP_0$ = 1130 μg L^{-1}; $HAAFP_0$ = 1906 μg L^{-1}; $AOXFP_0$ = 2840 μg eq. Cl L^{-1}.

Table 6
Characterization of surface water.

Parameter	Value
pH	7.8
Conductivity (μS cm^{-1})	252
Turbidity (NTU)	1.2
DOC (mg L^{-1})	5.0
IC (mg L^{-1})	19.8
TPhC (mg eq. phenol L^{-1})	0.16
A_{254nm}	0.079
SUVA (L mg DOC^{-1} m^{-1})	1.58
THMFP (μg L^{-1})	405
HAAFP (μg L^{-1})	354
AOXFP (μg eq. Cl L^{-1})	3040
Fe (mg L^{-1})	0.040
Mn (mg L^{-1})	<0.025
NO_3^- (mg L^{-1})	4.0
SO_4^{2-} (mg L^{-1})	28.3

In Fig. 7**(B)** SUVA is the specific absorption at 254 nm calculated from the absorbance at 254 nm per DOC. The initial average SUVA value was as high as 8.5 L mg^{-1} m^{-1} corresponding to commercial humic acid solution. Large values of SUVA indicate the presence of high concentrations of humic or fulvic-like structures, main precursors of THMs and HAAs [8,50]. It was observed the fastest elimination of SUVA for ozonation and photocatalytic ozonation also resulted in a high removal of THMFP and HAAFP (Fig. 8). The large increase of AOXFP removal through photocatalytic ozonation, however, can be related to the degradation of other non-aromatic or non-absorbing (at 254 nm) compounds precursors of different DBPs. When these treatments (ozonation and photocatalytic ozonation) were applied, the elimination of phenolic moieties measured as TPhC reached the lowest values (Fig. 7**(D)**).

3.4. Surface water treatment

The catalyst Gp-BM-LP was checked for treating real surface water. The main characteristics of the water sample are summarized in Table 6.

With respect to the NOM present in the surface water, it is noteworthy a low value of DOC with SUVA lower than for humic acid solutions, indicating the presence of other type of organic compounds. In fact, the contribution of THMFP and HAAFP barely accounts for 20 % of AOXFP, typical in surface waters of different sources [3]. The DBPs detected at higher concentrations after chlorination of raw surface water were CF and TCA.

Fig. 9 summarizes the main results for DOC and DBPFP removals through the ozonation-chlorination sequence of surface water. Dotted lines mark the necessary removal to reach the regulated limits for 4-THMs and 5-HAAs. As for humic acid study, the highest mineralization was obtained for the solar radiation assisted processes photolytic and photocatalytic ozonation, but contrarily, at 180 min of reaction, a detrimental effect was observed in DOC removal with the use of the catalyst (DOC removal percentages were 68 in O_3/rad vs. 48 % in photocatalytic ozonation with Gp-BM-LP catalyst). Besides, photolytic ozonation promoted the highest THMFP and HAAFP elimination, with the final effluent below the established limits. To go deeper in this behavior, Fig. 10 represents DOC profiles with time for photolytic and photocatalytic ozonation of surface water.

It can be observed a higher DOC removal through photocatalytic ozonation until 90 min compared to photolytic ozonation. However, from that time on, acceleration of the mineralization rate during photolytic ozonation is observed. Unlike what happens with humic acid in ultrapure water, this performance in surface water, apart from the moderate photocatalytic activity of the material, may also be related to the complex composition of the water matrix which can contain compounds that favors the photolysis of ozone or DOC such as some dissolved metallic ions (iron, manganese, etc.) or nitrates [53–55], among other species, being this ways more important than the heterogeneous catalysis.

In favor of the photocatalytic treatment, however, the elimination of DBPs' precursors other than those of THMs and HAAs was greatly improved reaching ca. 70 % removal of AOXFP. Then, although no reflected in the mineralization degree, if the global AOX parameter is considered, photocatalytic ozonation offers promising results, though to meet the regulation limits it would be easier to implement the photolytic ozonation treatment.

Finally, to check the stability of the material during photocatalytic ozonation, 3 consecutive runs were carried out during 90 min. The results of DOC and DBPFP removals with the results for photolytic ozonation at similar conditions for comparison are summarized in Fig. 11.

It can be noticed a stable performance of the catalyst during the 3 runs (4.5 h) with an AOXFP percentage removal higher than through 90

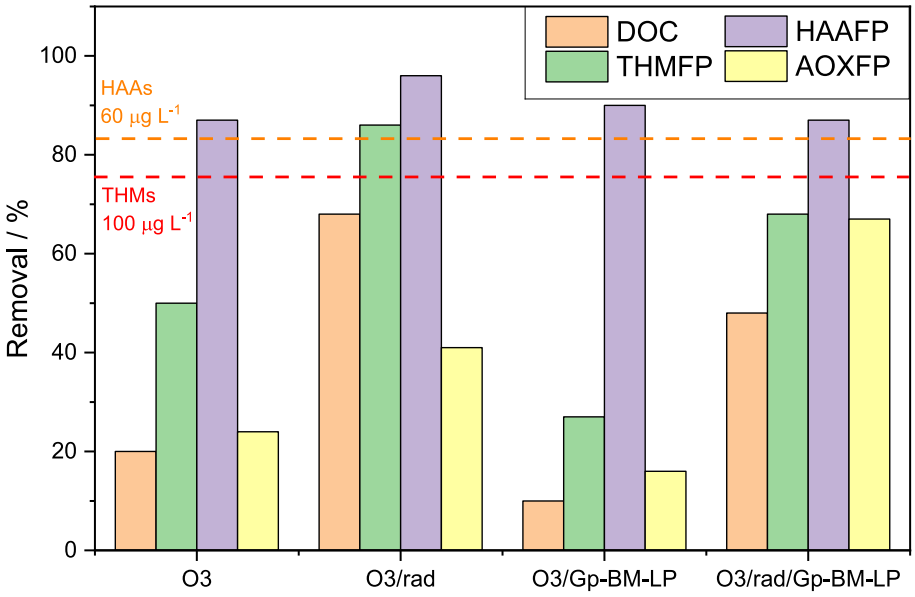

Fig. 9. DOC removal at 180 min of ozonation treatment and post-chlorination DBPFP elimination. Ozonation conditions: DOC_0 = 5.0 mg L^{-1}; C_{CAT} = 100 mg L^{-1}; C_{O3g} = 5 mg L^{-1}; Q = 10 L h^{-1}; pH_0 = 7.8; I_{irr} = 581 W m^{-2}; V = 0.5 L. Chlorination conditions: V = 125 mL; pH = 7.8; Cl_2/DOC > 15 mg/mg; $THMFP_0$ = 405 μgL^{-1}; $HAAFP_0$ = 354 μg L^{-1}; $AOXFP_0$ = 3040 μg eq. Cl L^{-1}.

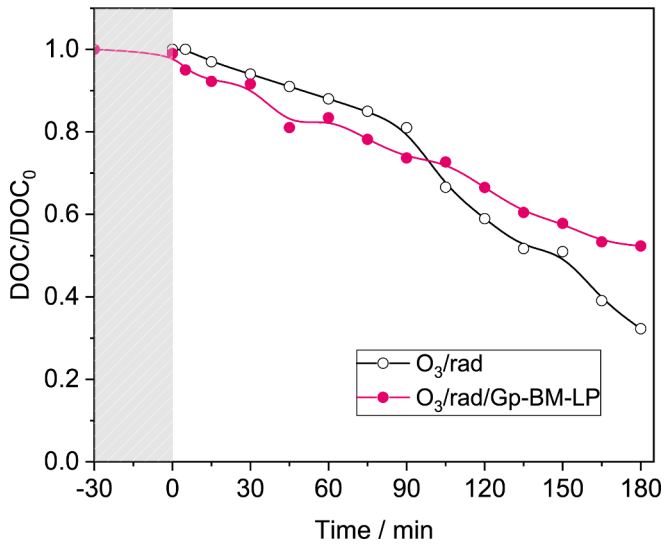

Fig. 10. DOC evolution during solar radiation ozonation treatments with the Gp-BM-LP catalyst. Ozonation conditions: DOC_0 = 5.0 mg L^{-1}; C_{CAT} = 100 mg L^{-1}; C_{O3g} = 5 mg L^{-1}; Q = 10 L h^{-1}; pH_0 = 7.8; I_{irr} = 581 W m^{-2}; V = 0.5 L.

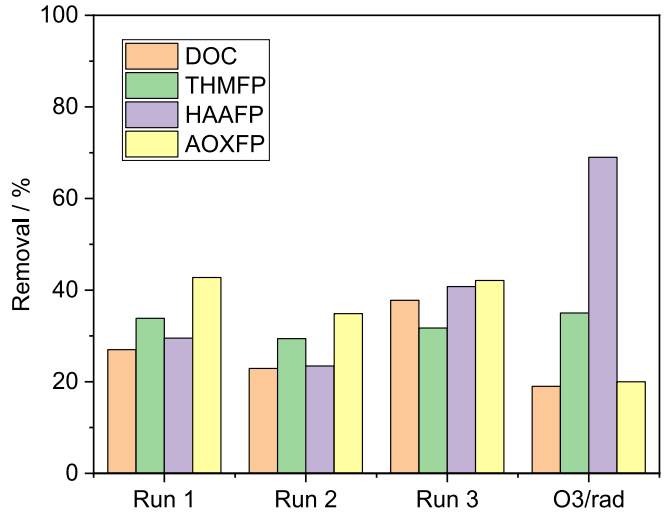

Fig. 11. DOC removal after 90 min of consecutive photocatalytic ozonation treatment and post-chlorination DBPFP elimination. Ozonation conditions: DOC_0 = 5.0 mg L^{-1}; C_{CAT} = 100 mg L^{-1}; C_{O3g} = 5 mg L^{-1}; Q = 10 L h^{-1}; pH_0 = 7.8; I_{irr} = 581 W m^{-2}; V = 0.5 L. Chlorination conditions: V = 125 mL; pH = 7.8; Cl_2/DOC > 15 mg/mg; $THMFP_0$ = 405 μg L^{-1}; $HAAFP_0$ = 354 μg L^{-1}; $AOXFP_0$ = 3040 μg eq. Cl L^{-1}.

min of photolytic ozonation and postchlorination. Even with the ozonation pre-treatment of Gp-BM-LP, the deactivation of the material in long-term experiments cannot be discarded. However, given its limited catalytic activity (and also the other carbon catalysts tested in this work), its combination with some active photocatalyst will be the subject of further work, thus additional studies on their long-term stability will be necessary.

4. Conclusions

From this work focused on the use of different carbon structures based on graphite, modified graphite, graphene and graphene oxide for the removal of disinfection by-products formation potential, the main conclusions reached are:

- The most effective treatment to increase the surface area of graphite, ball milling compared to potassium oxalate or ammonium nitrate, produced samples with some structural distortion breaking the particles through the in-plane graphene sheets (L_a) and through the staking height (L_c) also with graphene layers separation (d_{002}). The ozonation treatment of all carbon materials produced the generation of surface oxygen groups of acidic-type when ozonation is performed in liquid phase in contrast to the generation of more phenolic-like groups through ozonation in gas phase. However, no treatment achieved high exfoliation degree of the graphene layers of graphite to form graphene, oxidized graphene or graphene oxide.
- General positive effects of BET surface area, distortion degree and surface oxygen groups content were noticed in the catalytic activity of the materials. The highest catalytic activity during catalytic/photocatalytic ozonation was observed for commercial graphene and oxidized graphene, and for graphene oxide in dark conditions, however this did not result in a high DBPFP removal and some instability of the materials was demonstrated. With moderate catalytic activity but a high DBPFP removal, ball-milled graphite ozonated in liquid phase, was selected for photocatalytic ozonation of real surface water.
- Better results in AOXFP removal have been obtained through photocatalytic ozonation-chlorination sequence compared to the non-catalytic treatments. However, searching for more active and stable materials that promote higher mineralization will be continued in further works.

CRediT authorship contribution statement

M.A. Jiménez-López: Investigation, Validation, Writing – original draft, Resources. **A. Rey:** Conceptualization, Methodology, Formal analysis, Writing – review & editing, Supervision, Funding acquisition. **V. Montes:** Investigation, Validation, Funding acquisition. **F.J. Beltrán:** Conceptualization, Methodology, Writing – review & editing, Supervision, Project administration, Funding acquisition.

Declaration of Competing Interest

The authors declare that they have no known competing financial interests or personal relationships that could have appeared to influence the work reported in this paper.

Data availability

Data will be made available on request.

Acknowledgements

This research was funded by the Agencia Estatal de Investigación (AEI) of Spain through the projects PID2019-104429RB-I00/AEI/10.13039/501100011033 and CTQ2015-73168-JIN (AEI/FEDER/UE). Dr. V. Montes thanks Junta de Extremadura and European Regional Development Funds through the project IB20042. M.A. Jiménez-López thanks AEI for a FPI predoctoral grant PRE2020-091840. The authors also thank the SAIUEX service of the University of Extremadura for characterization analyses.

Appendix A. Supplementary material

Supplementary data to this article can be found online at https://doi.org/10.1016/j.seppur.2023.125156.

References

[1] S.D. Richardson, M.J. Plewa, To regulate or not to regulate? What to do with more toxic disinfection by-products? J. Environ. Chem. Eng. 8 (2020), 103939 https://doi.org/10.1016/j.jece.2020.103939.

[2] F.J. Beltrán, A. Rey, O. Gimeno, The role of catalytic ozonation processes on the elimination of DBPs and their precursors in drinking water treatment, Catalysts 11 (2021), https://doi.org/10.3390/catal11040521.

[3] S.D. Richardson, M.J. Plewa, E.D. Wagner, R. Schoeny, D.M. DeMarini, Occurrence, genotoxicity, and carcinogenicity of regulated and emerging disinfection by-products in drinking water: A review and roadmap for research, Mutat. Res. - Rev Mutat. Res. 636 (2007) 178–242, https://doi.org/10.1016/j.mrrev.2007.09.001.

[4] U. Von Gunten, Oxidation processes in water treatment: are we on track? Environ. Sci. Tech. 52 (2018) 5062–5075, https://doi.org/10.1021/acs.est.8b00586.

[5] A.A. Cuthbertson, S.Y. Kimura, H.K. Liberatore, R.S. Summers, D.R.U. Knappe, B. D. Stanford, J.C. Maness, R.E. Mulhern, M. Selbes, S.D. Richardson, Does granular activated carbon with chlorination produce safer drinking water? From disinfection byproducts and total organic halogen to calculated toxicity, Environ. Sci. Tech. 53 (2019) 5987–5999, https://doi.org/10.1021/acs.est.9b00023.

[6] R. Lamsal, M.E. Walsh, G.A. Gagnon, Comparison of advanced oxidation processes for the removal of natural organic matter, Water Res. 45 (2011) 3263–3269, https://doi.org/10.1016/j.watres.2011.03.038.

[7] B.K. Mayer, E. Daugherty, M. Abbaszadegan, Evaluation of the relationship between bulk organic precursors and disinfection byproduct formation for advanced oxidation processes, Chemosphere 121 (2015) 39–46, https://doi.org/10.1016/j.chemosphere.2014.10.070.

[8] G.A. De Vera, D. Stalter, W. Gernjak, H.S. Weinberg, J. Keller, M.J. Farré, Towards reducing DBP formation potential of drinking water by favouring direct ozone over hydroxyl radical reactions during ozonation, Water Res. 87 (2015) 49–58, https://doi.org/10.1016/j.watres.2015.09.007.

[9] U. Von Gunten, Ozonation of drinking water: Part II Disinfection and by-Product Formation in Presence of Bromide, Iodide or Chlorine, Water Res. 37 (2003) 1469–1487, https://doi.org/10.1016/S0043-1354(02)00458-X.

[10] F.J. Beltrán, Ozone Reaction Kinetics for Water and Wastewater Systems, CRC Press, Boca Raton, Florida, USA, 2004.

[11] J. Rivera-Utrilla, M.V. López-Ramón, M. Sánchez-Polo, M.Á. Álvarez, I. Velo-Gala, Characteristics and behavior of different catalysts used for water decontamination in photooxidation and ozonation processes, Catalysts 10 (2020) 1–66, https://doi.org/10.3390/catal10121485.

[12] F.J. Beltrán, P.M. Álvarez, O. Gimeno, Graphene-based catalysts for ozone processes to decontaminate water, Molecules 24 (2019), https://doi.org/10.3390/molecules24193438.

[13] M. Samriti, Z. Chen, S. Sun, J. Prakash, Design and engineering of graphene nanostructures as independent solar-driven photocatalysts for emerging applications in the field of energy and environment, Mol. Syst. Des. Eng. 7 (2022) 213–238, https://doi.org/10.1039/D1ME00179E.

[14] F. Bernat-Quesada, J.C. Espinosa, V. Barbera, M. Álvaro, M. Galimberti, S. Navalón, H. García, Catalytic ozonation using edge-hydroxylated graphite-based materials, ACS Sustain. Chem. Eng. 7 (2019) 17443–17452, https://doi.org/10.1021/acssuschemeng.9b04646.

[15] R. Yuan, B. Zhou, X. Zhang, H. Guan, Photocatalytic degradation of humic acids using substrate-supported Fe3+-doped TiO2 nanotubes under UV/O3 for water purification, Environ. Sci. Pollut. Res. 22 (2015) 17955–17964, https://doi.org/10.1007/s11356-015-4910-z.

[16] A.M. Chávez, A. Rey, F.J. Beltrán, P.M. Álvarez, Solar photo-ozonation: A novel treatment method for the degradation of water pollutants, J. Hazard. Mater. 317 (2016) 36–43, https://doi.org/10.1016/j.jhazmat.2016.05.050.

[17] E. Mena, A. Rey, B. Acedo, F.J. Beltrán, S. Malato, On ozone-photocatalysis synergism in black-light induced reactions: Oxidizing species production in photocatalytic ozonation versus heterogeneous photocatalysis, Chem. Eng. J. 204–205 (2012) 131–140, https://doi.org/10.1016/j.cej.2012.07.076.

[18] V. Gómez-Serrano, P.M. Álvarez, J. Jaramillo, F.J. Beltrán, Formation of oxygen structures by ozonation of carbonaceous materials prepared from cherry stones: II. Kinetic study, Carbon N. Y. 40 (2002) 523–529, https://doi.org/10.1016/S0008-6223(01)00142-7.

[19] V. Gómez-Serrano, P.M. Álvarez, J. Jaramillo, F.J. Beltrán, Formation of oxygen complexes by ozonation of carbonaceous materials prepared from cherry stones I. Thermal effects, Carbon N. Y. 40 (2002) 513–522, https://doi.org/10.1016/S0008-6223(01)00141-5.

[20] J. Rivera-Utrilla, M. Sánchez-Polo, V. Gómez-Serrano, P.M. Álvarez, M.C.M. Alvim-Ferraz, J.M. Dias, Activated carbon modifications to enhance its water treatment applications. An overview, J. Hazard. Mater. 187 (2011) 1–23, https://doi.org/10.1016/j.jhazmat.2011.01.033.

[21] A.E.D. Mahmoud, A. Stolle, M. Stelter, Sustainable synthesis of high-surface-area graphite oxide via dry ball milling, ACS Sustain. Chem. Eng. 6 (2018) 6358–6369, https://doi.org/10.1021/acssuschemeng.8b00147.

[22] C. Moreno-Castilla, M.A. Ferro-Garcia, J.P. Joly, I. Bautista-Toledo, F. Carrasco-Marin, J. Rivera-Utrilla, Activated carbon surface modifications by nitric acid, hydrogen peroxide, and ammonium peroxydisulfate treatments, Langmuir 11 (1995) 4386–4392, https://doi.org/10.1021/la00011a035.

[23] J.A. Menéndez, M.J. Illán-Gómez, C.A.L. y León, L.R. Radovic, On the difference between the isoelectric point and the point of zero charge of carbons, Carbon N. Y. 33 (1995) 1655–1657, https://doi.org/10.1016/0008-6223(95)96817-R.

[24] M.V. López-Ramón, F. Stoeckli, C. Moreno-Castilla, F. Carrasco-Marín, On the characterization of acidic and basic surface sites on carbons by various techniques, Carbon n. y. 37 (1999) 1215–1221, https://doi.org/10.1016/S0008-6223(98)00317-0.

[25] F.A. Amaringo Villa, Determinación del punto de carga cero y punto isoeléctrico de dos residuos agrícolas y su aplicación en la remoción de colorantes, Rev. Investig. Agrar. y Ambient. 4 (2013) 27, https://doi.org/10.22490/21456453.982.

[26] H. Bader, J. Hoigné, Determination of ozone in water by the indigo method, Water Res. 15 (1981) 449–456, https://doi.org/10.1016/0043-1354(81)90054-3.

[27] W. Masschelein, M. Denis, R. Ledent, Spectrophotometric determination of residual hydrogen peroxide, Water Sew. Work. 124 (1977).

[28] V.C. Hand, D.W. Margerum, Kinetics and mechanisms of the decomposition of dichloramine in aqueous solution, Inorg. Chem. 22 (1983) 1449–1456, https://doi.org/10.1021/ic00152a007.

[29] M.J. Cardador, A. Serrano, M. Gallego, Simultaneous liquid–liquid microextraction/methylation for the determination of haloacetic acids in drinking waters by headspace gas chromatography, J. Chromatogr. A 1209 (2008) 61–69, https://doi.org/10.1016/j.chroma.2008.09.033.

[30] K.S.W. Sing, Reporting physisorption data for gas/solid systems with special reference to the determination of surface area and porosity (Recommendations 1984), 57 (1985) 603–619, doi: 10.1351/pac198557040603.

[31] P. Krawczyk, Effect of ozone treatment on properties of expanded graphite, Chem. Eng. J. 172 (2011) 1096–1102, https://doi.org/10.1016/j.cej.2011.06.005.

[32] H. Valdés, M. Sánchez-Polo, J. Rivera-Utrilla, C.A. Zaror, Effect of ozone treatment on surface properties of activated carbon, Langmuir 18 (2002) 2111–2116, https://doi.org/10.1021/la010920a.

[33] Y. Wang, Y. Xie, H. Sun, J. Xiao, H. Cao, S. Wang, Efficient catalytic ozonation over reduced graphene oxide for p-hydroxylbenzoic acid (PHBA) destruction: active site and mechanism, ACS Appl. Mater. Interfaces 8 (2016) 9710–9720, https://doi.org/10.1021/acsami.6b01175.

[34] P.M. Álvarez, J.F. García-Araya, F.J. Beltrán, F.J. Masa, F. Medina, Ozonation of activated carbons: Effect on the adsorption of selected phenolic compounds from aqueous solutions, J. Colloid Interface Sci. 283 (2005) 503–512, https://doi.org/10.1016/j.jcis.2004.09.014.

[35] J. Jaramillo, P.M. Álvarez, V. Gómez-Serrano, Oxidation of activated carbon by dry and wet methods: Surface chemistry and textural modifications, Fuel Process. Technol. 91 (2010) 1768–1775, https://doi.org/10.1016/j.fuproc.2010.07.018.

[36] A.A. Moosa, Z.H. Mahdi, M.A. Mutar, Preparation of graphene oxide from expanded graphite at different microwave heating times, J. Eng. Technol. Sci. 53 (2021), https://doi.org/10.5614/j.eng.technol.sci.2021.53.3.5.

[37] A. Kaushal, S.K. Dhawan, V. Singh, Determination of crystallite size, number of graphene layers and defect density of graphene oxide (GO) and reduced graphene oxide (RGO), AIP Conf. Proc. 2115 (2019) 1–5, https://doi.org/10.1063/1.5112945.

[38] T. Qiu, J.G. Yang, X.J. Bai, Y.L. Wang, The preparation of synthetic graphite materials with hierarchical pores from lignite by one-step impregnation and their characterization as dye absorbents, RSC Adv. 9 (2019) 12737–12746, https://doi.org/10.1039/c9ra00343f.

[39] D. López-Díaz, M. López Holgado, J.L. García-Fierro, M.M. Velázquez, Evolution of the Raman spectrum with the chemical composition of graphene oxide, J. Phys. Chem. C 121 (2017) 20489–20497, https://doi.org/10.1021/acs.jpcc.7b06236.

[40] M. González-Barriuso, A. Yedra, P. Mantilla, C. Manteca-Martínez, Synthesis and characterisation of reduced graphene oxide from graphite waste and HOPG, Mater. Res. Innov. 19 (2015) 192–195, https://doi.org/10.1179/1433075X14Y.0000000241.

[41] S. Claramunt, A. Varea, D. López-Díaz, M.M. Velázquez, A. Cornet, A. Cirera, The importance of interbands on the interpretation of the raman spectrum of graphene oxide, J. Phys. Chem. C 119 (2015) 10123–10129, https://doi.org/10.1021/acs.jpcc.5b01590.

[42] R. Muzyka, S. Drewniak, T. Pustelny, M. Chrubasik, G. Gryglewicz, Characterization of graphite oxide and reduced graphene oxide obtained from different graphite precursors and oxidized by different methods using Raman spectroscopy, Materials (basel). 11 (2018) 15–17, https://doi.org/10.3390/ma11071050.

[43] C. Moreno-Castilla, F. Carrasco-Marín, F.J. Maldonado-Hódar, J. Rivera-Utrilla, Effects of non-oxidant and oxidant acid treatments on the surface properties of an activated carbon with very low ash content, Carbon n. y. 36 (1998) 145–151, https://doi.org/10.1016/S0008-6223(97)00171-1.

[44] M. Pakuła, A. Świątkowski, M. Walczyk, S. Biniak, Voltammetric and FT-IR studies of modified activated carbon systems with phenol, 4-chlorophenol or 1,4-benzoquinone adsorbed from aqueous electrolyte solutions, Colloids Surfaces A Physicochem. Eng. Asp. 260 (2005) 145–155, https://doi.org/10.1016/j.colsurfa.2005.03.013.

[45] L.M. Pastrana-Martínez, S. Morales-Torres, V. Likodimos, P. Falaras, J. L. Figueiredo, J.L. Faria, A.M.T. Silva, Role of oxygen functionalities on the synthesis of photocatalytically active graphene-TiO_2 composites, Appl. Catal. B Environ. 158–159 (2014) 329–340, https://doi.org/10.1016/j.apcatb.2014.04.024.

[46] J.L. Figueiredo, M.F.R. Pereira, M.M.A. Freitas, J.J.M. Órfão, Modification of the surface chemistry of activated carbons, Carbon n. y. 37 (1999) 1379–1389, https://doi.org/10.1016/S0008-6223(98)00333-9.

[47] H.P. Boehm, Some aspects of the surface chemistry of carbon blacks and other carbons, Carbon n. y. 32 (1994) 759–769, https://doi.org/10.1016/0008-6223(94)90031-0.

[48] J. Agbaba, J. Molnar, A. Tubic, M. Watson, S. Maletic, B. Dalmacija, Effects of water matrix and ozonation on natural organic matter fractionation and corresponding disinfection by-products formation, Water Sci. Technol Water Supply 15 (2015) 75–83, https://doi.org/10.2166/ws.2014.086.

[49] F.J. Beltrán, M. González, J.F. García-Araya, J.L. Cabrera, The use of ozonation to reduce the potential for forming trihalomethane compounds in chlorinating resorcinol, phloroglucinol and 1,3 cyclohexanedione, Chem. Eng. Commun. 96 (1990) 321–339, https://doi.org/10.1080/00986449008911499.
[50] G. Hua, D.A. Reckhow, Characterization of disinfection byproduct precursors based on hydrophobicity and molecular size, Environ. Sci. Tech. 41 (2007) 3309–3315, https://doi.org/10.1021/es062178c.
[51] A.M. Dimiev, L.B. Alemany, J.M. Tour, Graphene oxide, origin of acidity, its instability in water, and a new dynamic structural model, ACS Nano. 7 (2013) 576–588, https://doi.org/10.1021/nn3047378.
[52] F. Yang, M. Zhao, Z. Wang, H. Ji, B. Zheng, D. Xiao, L. Wu, Y. Guo, The role of ozone in the ozonation process of graphene oxide: Oxidation or decomposition? RSC Adv. 4 (2014) 58325–58328, https://doi.org/10.1039/c4ra08750j.
[53] M.W. Lam, K. Tantuco, S.A. Mabury, PhetoFate: a new approach in accounting for the contribution of indirect photolysis of pesticides and pharmaceuticals in surface waters, Environ. Sci. Tech. 37 (2003) 899–907, https://doi.org/10.1021/es025902+.
[54] A. Espejo, F.J. Beltrán, F.J. Rivas, J.F. García-Araya, O. Gimeno, Iron-based catalysts for photocatalytic ozonation of some emerging pollutants of wastewater, J. Environ. Sci. Heal. Part A, Toxic/Hazardous Subst. Environ. Eng. 50 (2015) 553–562, https://doi.org/10.1080/10934529.2015.994939.
[55] E.M. Rodríguez, G. Fernández, P.M. Alvarez, F.J. Beltrán, TiO2 and Fe (III) photocatalytic ozonation processes of a mixture of emergent contaminants of water, Water Res. 46 (2012) 152–166, https://doi.org/10.1016/j.watres.2011.10.038.